USING COLOUR FEATURES TO CLASSIFY OBJECTS AND PEOPLE IN A VIDEO SURVEILLANCE NETWORK

By

Mathew Price

Supervised by

Prof. Gerhard De Jager and Dr Fred Nicolls

SUBMITTED IN FULFILLMENT OF THE
REQUIREMENTS FOR THE DEGREE OF
MASTER OF SCIENCE
AT
UNIVERSITY OF CAPE TOWN
CAPE TOWN, SOUTH AFRICA
MARCH 31 2004

Acknowledgements

This project would not have succeeded without the support of my supervisors, Prof. Gerhard de Jager and Dr Fred Nicolls (reader extraordinaire). In addition, I would like to thank TSS Technology (De Beers) and the National Research Foundation for financial support. Thanks to Bruno Merven (my office neighbour) for the late night support and my parents for tolerating my anti-social behaviour for the past three months.

Finally, a huge thank you to Markus 'legend' Louw who painstakingly hand-segmented over 600 frames of video (first two test sequences) so that ground truth measurements were available.

Abstract

Visual tracking of humans has proved to be an extremely challenging task for computer vision systems. One idea towards the development of these systems is the incorporation of colour. Often the colour appearance of a person can provide enough information to identify an object or person in the short-term. However, the imprecise nature of colour measurements typically encountered in image processing has limited their use. This thesis presents a system which uses the colour appearances of objects and people for tracking across multiple camera views in a digital video surveillance network. A distributed framework for creating and sharing visual information between several cameras is suggested, including a simple method for generating relative colour constancy. Tracking has been approached from a classification standpoint allowing the system to cope with multiple occlusions, variable camera pose, and asynchronous video feeds. Several test cases exhibiting various surveillance scenarios are used to assess system performance, which is determined via some well-known surveillance metrics. The system exhibits an average tracker detection rate of approximately 80% with a false alarm rate of less than 2%. It is envisaged that the combination of the presented system and motion estimation tracking techniques could eventually result in a robust, real-time tracking system.

Table of Contents

List of Tables

List of Figures

Chapter 1

Introduction

As digital cameras become increasingly small and less expensive, there is a thrust towards their integration with everyday living. Combined with the processing speeds of modern computers, many visual tasks previously considered only capable by humans are now becoming automated. Development of such systems has spawned much research in the area of machine perception and has been aptly termed — Computer Vision.

Object tracking is one such area which has drawn a large interest. This is primarily because of the wide range of applications it encompasses. Some of these include: detection of stationary objects in airports and train stations (security threats); recognition of human actions; automatic commentary of sports matches; automated person surveillance for CCTV networks; personal positioning; and vehicle license plate tracking.

The context of tracking selected in this thesis applies to the area of computer-aided surveillance. Large buildings regularly use CCTV networks to monitor the movements of people in order to provide security and safety. This leads to a bottleneck of information since an operator can only manage a finite number of camera views accurately at one time. The idea of computer-aided surveillance fits into the intermediatory role of filtering out uninteresting events and drawing the operators' attention

to items of specific importance (eg. people accessing restricted areas). Therefore, a basic requirement of such a system is the ability to keep track of several people simultaneously, especially their transitions between different camera views.

1.1 Problem Definition

One interesting problem that arises, is the issue of tracker initialisation. Many predictive tracking techniques have been developed, however, a common weakness in many of these systems is their dependence on parameter initialisation. Since a prediction is based on a current assumption and a noisy observation, errors are cumulative and can lead to eventual target loss. Recovery then requires that the tracker be re-initialised to the target's current position. The framework of tracking systems often does not allow for this.

The system proposed here approaches the tracking problem from a classification standpoint. Often the colour appearance of a person can provide enough information to determine their identity and thus their position in the short-term. Therefore, by modelling this colour appearance as a set of features, colour matching can be used to build a likelihood response to the model's spatial position in an arbitrary image. This one-shot style of tracking has the advantage of being able to deal with occluding objects, movement between multiple camera views and asynchronous video feeds. In addition, the framework is extremely flexible, allowing optional integration with a variety of information such as camera pose, geometric features and motion tendencies.

1.2 Objectives

The primary objective of this work is to determine the limits of using colour information in surveillance tracking. It was envisioned that such a system, focusing solely on visual object features, could then be merged with robust motion estimation techniques to provide a solid tracking framework suitable for use in a large surveillance

network. These objectives prompted the development of a distributed framework which can be optimised later for real-time operation.

1.3 Layout of document

This document is structured in a manner that allows the reader to be introduced to topics in context while preserving the temporal structure of data flow through the system. For this reason, the *Background*, **Chapter 2**, only covers a few global areas. Further theory for each sub-system is then contained in the introductory sections of subsequent chapters.

The system framework is introduced in the *Architectural Overview*, **Chapter 3**, which motivates the approach and summarises the system structure and data flow. Each sub-system is then discussed in **Chapters 4, 5, 6** and **7**. The arrangement of these chapters follows a: Descriptive theory; Implementation; and Limitations format. The descriptive theory systematically derives sub-system concepts while the implementation and limitations sections describe the realistic customisations specific to coding and operation.

Results are compiled for three test cases in **Chapter 8**. Firstly, the assessment method is described followed by a detailed analysis of the system performance versus parameter selection. The three test cases are then dealt with separately, concluding with an overall system performance summary.

Finally, **Chapter 9** concludes the document with a brief final overview. The appendices consist of: An overview of SOM training (**Appendix A**); a specification of the test platform used (**Appendix B**); and a digital appendix (**Appendix C**) which refers to the accompanying CDROM. The digital appendix provides the video sequences for each test case as well as the set of colour trajectory images for each test subject. The original Acrobat PDF document is also included should any printed colour diagrams seem unclear.

Chapter 2

Background

This project was initiated from the growing need of digital surveillance systems to perform computer-aided monitoring. Specifically, the idea of classification based on colour features arose from a previous project in which an on-body camera was used as a personal positioning device. The variable camera pose and real-time constraints of that system did not allow conventional methods such as background segmentation and 3-D pose reconstruction to be applied. This therefore preempted the shift towards a more featurised and matching-orientated approach.

The work presented in this thesis focuses on fast, reliable recognition of an object or person's position in a scene via the matching of colour features. The following sections aim to provide a broad background within the context of tracking, colour imaging and data clustering techniques.

2.1 Tracking Approaches

In the global sense, tracking refers to pin-pointing the position of a target object with respect to some reference at any time. Many different levels of tracking have been addressed by vision systems, each requiring a different approach. To name but a few:

Articulate motion: The primary interest here is the accurate recording of a person's body movements. This has applications in detailed surveillance systems as well as medical research and automated understanding of body language (eg. gesture recognition and gait analysis) [34, 20].

Positioning: The aim in a positioning system is to track object positions with respect to their environment. This is classically of interest to the surveillance community and it represents a very generalised form of tracking.

Detection: Many tracking systems are dependent on the location of a particular object or body part (eg. animal, box, head, face). Detection methods aim to provide fast, robust methods for locating such items in an image. These are normally incorporated into larger systems (eg. [44]).

Robot vision: This arena encompasses a wide variety of methods geared towards creating autonomous robotic visual systems which mimic human traits. While the overall tasks are generally simpler (since they must be implemented in standalone hardware), the methods developed are extremely robust and applicable in a number of other systems (eg. [5]).

In terms of the generalised surveillance tracking class, which is the focus of this thesis, a number of alternative approaches have been explored. The continual innovation in this area is attributed to the quest to find the ultimate system which is both robust and capable of real-time operation.

A well known colour tracking method involves the use of the mean-shift method [7]. This approach uses a histogram-based search which iteratively finds the most similar target candidate using a histogram similarity metric based on the Bhattacharyya coefficient. Its primary advantage is its low computational complexity and near real-time operation. However in the long-term, histogram modelling methods have been known to fail (even with adaptation). Also, the scaling of models for multiple objects and camera views is awkward.

Motion estimation techniques such as Kalman [45] and particle filters [19] approach the tracking problem from a stochastic point of view. If objects are parameterised by their physical interactions with an environment, and these parameters are assumed to follow a basic motion model corrupted by some noise, then predictive estimates can be used to track each target's position in the context of its model. An advantage of this formulation is that it intuitively facilitates integration with 3-D based information. Both Kalman and condensation trackers have been applied to solving the multi-view correspondence tracking problem [27, 28, 30, 49]. However, performance is dependent on the number of objects and views in the scene as well as the initialisation process. It is for integration with such systems that this work was aimed.

Simpler approaches such as blob tracking using segmented masks combined with complex rule sets have also been attempted [25] with some good short-term results. Solving the problem of computational complexity within high dimensional parameter spaces, inconsistency of multiple camera hardware, and the lack of a standardised framework have kept tracking at the forefront of computer vision research.

2.2 Colour

A primary aspect of this thesis is the use of colour matching in digital video. Since the aim is to create a system that mimics the way humans discriminate objects based on colour, it is important to understand the underlying processes of human perception and how it relates to digital imaging.

2.2.1 Physical Colour

The visual spectrum for humans ranges from 400 nm (violet) to 700 nm (red) with a maximum sensitivity to wavelengths in the 550 nm (green) band [13]. Surfaces appear coloured as a result of several complex mechanisms which dictate how they transmit, reflect, absorb and scatter various frequencies of visible light. As a common example,

the green surface in Figure 2.1 is illuminated by a pure white light source. The surface absorbs most of the incident frequencies and reflects those in the middle of the visual spectrum (green). Since an observer looking at the surface will see only the reflected light, the surface will appear green. Had the illuminating source been pure red, on the other hand, the surface would have appeared black due to the absence of any green light for the surface to reflect.

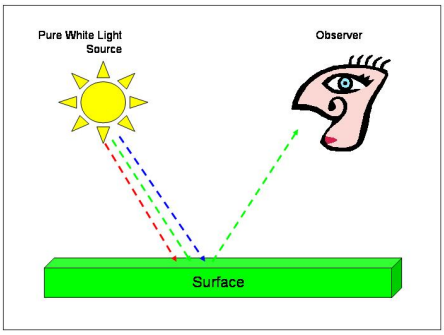

Figure 2.1: *Surface colour example.*

Generally, surfaces are more complicated than in the illustration. Angles of incidence and reflection as well as surface shape and material composition play vital roles in determining the quantities of spectral reflectance. The need to be able to predict the relationship between incident source light and reflected light on a general surface has led to the use of Bidirectional Reflectance Distribution Functions (*BRDF*). The amount of light energy travelling in a specified direction, per unit time, per unit area perpendicular to the direction of propagation, is known as *radiance* [15]. Its counterpart, *irradiance*, is defined as the incident power per unit area not foreshortened [15] (i.e. not perpendicular to the direction of propagation). The *BRDF* thus charts the ratio of outgoing radiance to incident irradiance. Simply put, a BRDF maps the incoming to outgoing direction of light of all visible frequencies for a particular surface.

In colour imaging, it is convenient to know whether the pixel value represents a true reading from a surface or whether it has been produced by some sort of lighting artifact. This knowledge would be especially useful, for instance, if one wanted to

normalise the lighting conditions between two images in order to compare object colours. Since the resulting image is a superposition of many processes, it is not possible to fully separate each process without extensive analysis of the relevant BRDFs (assuming they were available). For this reason, a common adopted practice is to represent the surface as a combination of its Lambertian and Specular components, which provide a good approximation for a variety of surfaces.

Lambertian or ideal diffuse surfaces describe a special class of surfaces whose reflectance is independent of the lighting direction. Examples of such surfaces include carpets, cotton cloth and matte painted surfaces. A second group of special surfaces are the specular or mirrored surfaces. Ideal specular surfaces reflect incoming light about the surface normal at the point of incidence. Generally, ideal specular surfaces are not overtly common, though many surfaces exhibit specular effects, eg. shiny metals and plastics. Typically, these surfaces will absorb some light (they are not perfect reflectors) and cause a variance in the direction of reflection. This produces a specular lobe or blurring effect. Narrow lobes result in bright specular highlights, while wider lobes relate to a dull, blurred reflections.

2.2.2 Human Vision

The human sensation of colour has been explained by the receptivity of cone cells in the retina to a particular frequency of light. Initially it was thought that there were thousands of types of cone cells, each sensitive to a particular colour, until Thomas Young introduced the trichromatic model in 1802 [22]. His theory proposed that all visible colours can be constructed from a mixture of three basic primaries: red; green; and blue.

Psychophysical experiments conducted by Helmholtz and Maxwell in the mid 19th century seemed to support Young's trichromatic representation. The theory was further confirmed in 1964 when microspectrometry identified the presence of three types of cone cells [46]: S-Cones; M-Cones and L-Cones (short, medium and long wavelength). The spectral response of these cones peak at 440 nm (Blue), 545 nm

(Green) and 565 nm (Red) respectively.

Though trichromatic theory validated the composition of colours via the three primaries, it did not fully explain the abstract process of colour perception. For instance, the combination of red and green light does not produce a reddish-green as one would think, but yellow [22]. Another anomaly is the blue after-effect one experiences after begin subjected to a prolonged yellow stimulus. These effects led to the proposal of the Opponent Colour theory in 1872 by physiologist Ewald Hering. Hering believed that there were in fact four unique colours — red, green, blue and yellow — and that perceived colours were produced by the opponent-processes of three colour channels, namely red-green, blue-yellow and black-white.

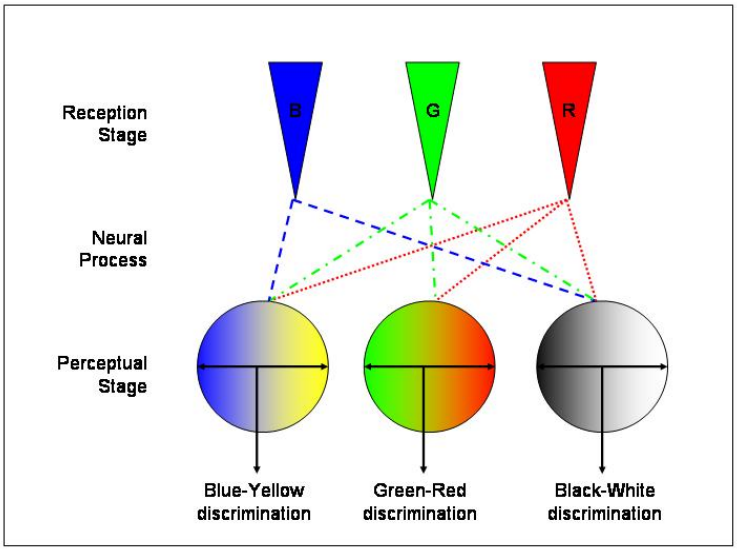

Figure 2.2: *Stage model for human colour perception.*

The fact that both theories contain truth — trichromatic theory is physically proven while the opponent colour theory explains the oddities of human perception — has led to the modern stage theory which combines both representations [22]. Colour vision is split into two stages as demonstrated in Figure 2.2. The first stage involves physical reception to an external stimulus by the three types of cone cells in the retina. These responses are then transformed by a neural process into the opponent colour signals which are then used for discrimination by the brain. The stage theory is therefore

able to explain the trichromatic nature of the human eye while also accounting for the perceptual sensations humans experience.

2.2.3 Colour Spaces

A linear colour space is a 3-D subspace of co-ordinates that describes a particular subset (*gamut*) of visible colours [15]. Colours are matched by the weighted sum of the three primaries. The weights required in order to match a particular colour are given by a set of colour matching functions (one for each primary). These colour matching functions are derived by experimental tuning of the weights of each primary to match each wavelength of unit radiance in the spectrum [15].

Depending on the application, it is convenient to be able to represent colour data in various ways. This has led to a vast number of differing colour spaces, each with its own primaries and colour matching functions.

RGB

Widely used to drive colour CRT displays as well as raster graphic systems, RGB has become an indispensable device colour system [13]. Colours are represented by the additive combination of red, green and blue primaries. The R, G, B values generally range from 0 to 255, forming a cube in cartesian co-ordinates (Figure 2.3). Thus each colour channel occupies 1 byte or 8 bits in digital media resulting in a 24 bit colour system.

It is unlikely that RGB image measurements of an object will remain constant over an extended period. This is primarily due to changes in ambient lighting and environmental positioning. It is therefore convenient to have an invariant which encapsulates the chromaticity of the object independent of lighting conditions. This introduces the notion of chromaticity co-ordinates for a colour space, in which the chromaticity is given by the normalisation of the true values. In RGB, this transformation results

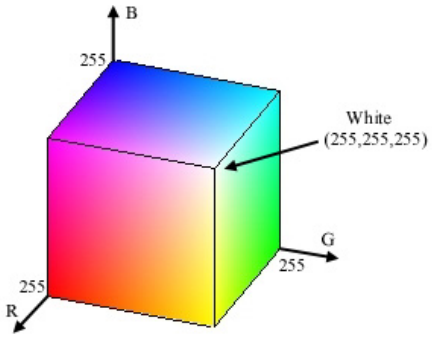

Figure 2.3: *RGB Cube.*

in the rgG space where chromaticity is given by the uncapitalised variables r and g, and G corresponds to the overall intensity. If a pixel has RGB values R, G and B, the rgG conversion is given by [14]:

$$r = \frac{R}{R+G+B} \tag{2.1}$$

$$g = \frac{G}{R+G+B} \tag{2.2}$$

$$G = 0.30R + 0.59G + 0.11B. \tag{2.3}$$

The b (blue chromaticity) fraction is omitted in rgG, since the normalisation implies that $r + g + b = 1$ and therefore the third value can be inferred from the other two.

HSV

In contrast to the RGB space, which is orientated to hardware, the HSV (Hue Saturation Value) model is derived from appearance to users. Closely related to the Munsell system, HSV uses cylindrical co-ordinates to describe tint, shade and tone [13].

The three perceptual attributes of human colour vision which make up the HSV space are:

Hue: An angle representing the wavelength (colour) of the illuminant. Hue values range from 0° (red) to 120° (green) to 240° (blue). Complementary colours then fall uniformly between the primaries (60° out of phase).

Saturation: The purity or the radial distance from the unsaturated white point. The values for saturation span from 0 (white) to 1 (pure Hue).

Value: Sometimes also referred to as Brightness, the Value represents the luminosity of the colour, which ranges from 0 (black) to 1 (white).

The HSV space thus forms the hexcone depicted in Figure 2.4. Chromaticity in the HSV space is intrinsically encapsulated by the HS components. However, care must be taken since Hue is undefined for zero Saturation. This causes noisy chromaticity measurements in image areas which are excessively bright or dark.

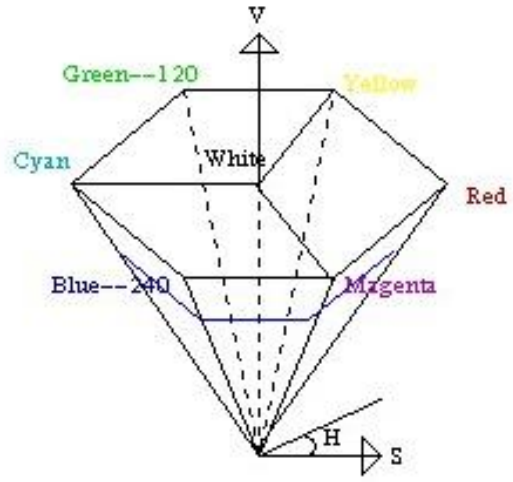

Figure 2.4: *HSV hexcone.*

CIE XYZ

In 1931, the Commission Internationale d'Elairage (CIE) introduced a representation which has become the governing standard for colour matching [13]. This representation was conceived in order to provide a model able to intuitively represent all visible

colours, thus dealing with the 'negative colours' phenomenon.

Inconveniently, positive RGB mixtures cannot match the entire range of visible colours in the spectrum. Newton's colour circle, shown in Figure 2.5, demonstrates why this is so, by showing the primaries required to match a 500 nm wavelength[22]. An additive combination of blue and green will produce a desaturated result. Therefore in order to match the colour correctly, a negative red stimulus must be added (which is impossible for CRT devices to achieve).

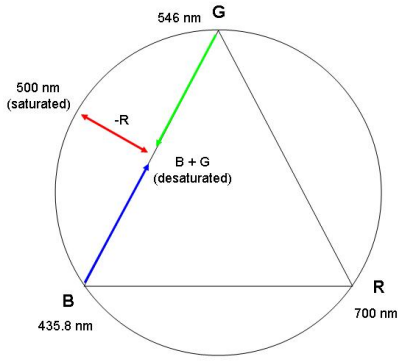

Figure 2.5: *Matching 500 nm wavelength using Newton's colour circle.*

The 1931 CIE XYZ space was therefore devised by defining imaginary primaries X, Y, and Z so that all visible wavelengths could be matched with positive mixtures. The transformation from RGB to CIE XYZ maps the RGB cube to the cone-shaped volume shown in Figure 2.6 by the transformation:

$$\begin{bmatrix} X \\ Y \\ Z \end{bmatrix} = \begin{bmatrix} 0.412452 & 0.357580 & 0.180423 \\ 0.212671 & 0.715160 & 0.072169 \\ 0.019334 & 0.119193 & 0.950227 \end{bmatrix} \begin{bmatrix} R \\ G \\ B \end{bmatrix} \tag{2.4}$$

The CIE chromaticity co-ordinates (x, y, z) [48] are further generated similar to the rgG transformation (Equation 2.5), forming the xy chromaticity plane shown in

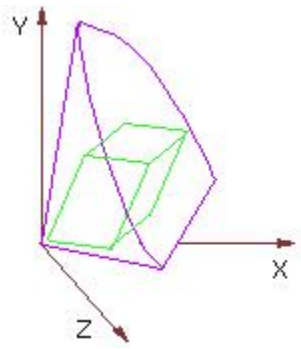

Figure 2.6: *CIE Colour Space w.r.t. RGB cube.*

Figure 2.7.

$$\mathrm{x} = \frac{X}{X+Y+Z},\ \mathrm{y} = \frac{Y}{X+Y+Z},\ \mathrm{z} = 1 - \mathrm{x} - \mathrm{y} \tag{2.5}$$

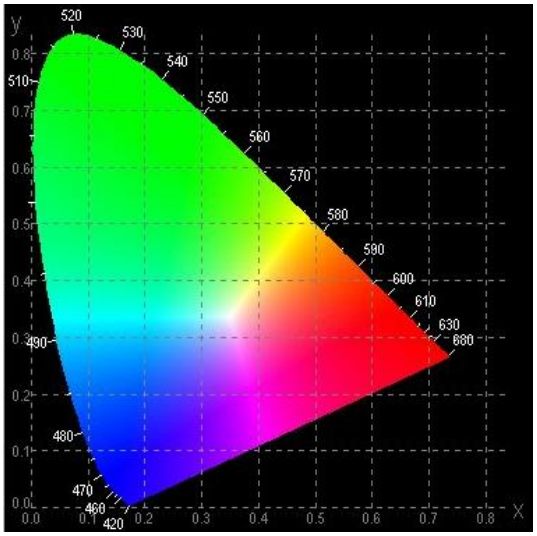

Figure 2.7: *CIE chromaticity diagram.*

A line between points in the CIE chromaticity diagram relates to all available colours between each endpoint. Furthermore, the colours within a triangle created by three points in the plane represent the gamut of colours that is available to the set of primaries defined by the vertices. This means that the CIE XYZ space is intrinsically

device independent and can be used to compare (or map) gamut regions between different devices.

CIE L*a*b*

While the CIE xy chromaticity diagram has useful properties for relating gamuts between various systems, it does not provide a qualitative measure for colour comparison. This lead to the definition of several other colour spaces which were geared to perceptual uniformity.

One of the most successful uniform colour spaces proposed was the 1976 CIE L*a*b* or CIELAB space [46]. The CIELAB definition is closely related to the opponent theory of colour vision. Forming a sphere (Figure 2.8), the space consists of two colour axes $a*$ $b*$ and a luminance $L*$ or brightness axis. The $a*$ values range from red to green, while the $b*$ values describe blue to yellow (opponent channels).

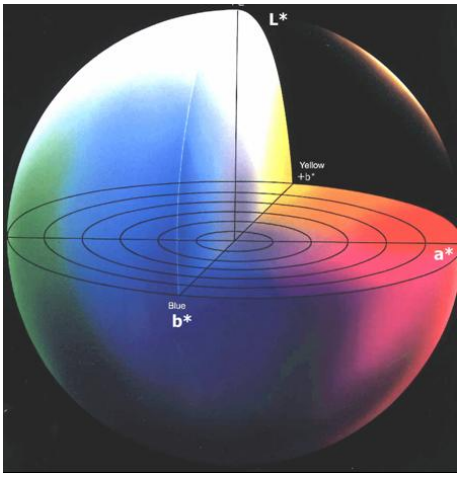

Figure 2.8: *CIE L*a*b* colour sphere.*

The L*, a*, and b* quantities are obtained by a transformation (Equations 2.6 to 2.9) of the CIE XYZ primaries normalised to a reference white point X_n, Y_n, Z_n (normally D65 for general daylight) [46].

$$\text{L}^* = \begin{cases} 116(\frac{Y}{Y_n})^{\frac{1}{3}} - 16 & if\ \frac{Y}{Y_n} > 0.008856 \\ 903.3(\frac{Y}{Y_n})^{\frac{1}{3}} - 16 & if\ \frac{Y}{Y_n} \leq 0.008856 \end{cases} \tag{2.6}$$

$$\text{a}^* = 500\left[f\left(\frac{X}{X_n}\right) - f\left(\frac{Y}{Y_n}\right)\right] \tag{2.7}$$

$$\text{b}^* = 200\left[f\left(\frac{Y}{Y_n}\right) - f\left(\frac{Z}{Z_n}\right)\right] \tag{2.8}$$

$$f(t) = \begin{cases} t^{\frac{1}{3}} & if\ t > 0.008856 \\ 7.787t + \frac{16}{116} & if\ t \leq 0.008856 \end{cases} \tag{2.9}$$

By definition, a perceptually uniform space means that colour differences between points in the space are directly proportional to the Euclidean distance measure. Thus for CIELAB points $(L*_1, a*_1, b*_1)$ and $(L*_2, a*_2, b*_2)$, the difference in colour stimuli $\Delta E*$ is:

$$\Delta E*^2 = (L*_1 - L*_2)^2 + (a*_1 - a*_2)^2 + (b*_1 - b*_2)^2. \tag{2.10}$$

If a more descriptive colour difference is required, the suggestion has been to use the $L*C*_{ab}H*_{ab}$ representation instead [46]. Basically, CIELCH is the polar coordinate equivalent of CIELAB. $L*$ remains as the brightness measure, while the a*-b* plane is replaced by chroma $C*_{ab}$ (comparable to saturation) and hue component $H*_{ab}$. The descriptive colour differences between points $(L*_1, C*_{ab_1}, H*_{ab_1})$ and $(L*_2, C*_{ab_2}, H*_{ab_2})$ are then given by the three quantities [46]:

$$\Delta L* = L*_2 - L*_1 \tag{2.11}$$

$$\Delta C* = C*_{ab_2} - C*_{ab_1} \tag{2.12}$$

$$\Delta H* = \sqrt{(\Delta a*)^2 + (\Delta b*)^2 - (\Delta C*)^2}. \tag{2.13}$$

where $\Delta a*$ and $\Delta b*$ are the component differences in the a*-b* plane.

2.2.4 Colour difference metrics

The nature of an image processing system determines the type of colour model applied. For instance, an application requiring a descriptive difference between colours implies that a perceptually uniform colour space should be used.

The previous section described the 1976 CIELAB space which allows the Euclidean distance between points to be used as a colour difference metric. Unfortunately, further experiments have proved that CIELAB is not completely uniform [46] and does not provide a consistently good measure of the magnitude of perceptual difference between stimuli. This has lead to the definition of other, more optimised metrics such as CMC (British standard BS:6923), M&S (1980 Marks & Spencer equations for textile industry), BFD (refined CMC equations), and CIE 94 (simplified CMC version).

While it has not been proved whether any of these new metrics are better than the other, the British CMC equation, which uses user-configurable tolerance ellipsoids, is currently being considered as an ISO standard.

In the context of this thesis, exact colour differences were not critical to operation (since camera noise distorts image quality in any case). Therefore CIELAB, which is computationally simpler and more intuitive for spherical feature spaces, was selected.

2.3 Clustering

Discriminative classification methods generally conform to either a *supervised* or *unsupervised* approach [10]. Supervised methods require the structure and pattern of the presented data to be pre-defined so that the optimum boundaries can be decided. On the other hand, unsupervised methods are used in order to seek out and discover the intrinsic patterns for themselves.

Clustering refers to a set of unsupervised learning algorithms which partition featurised data based on their spatial coherence in the feature space. Clustering methods are therefore dependent on the separability of pattern features and the type of distance metric being applied. Two main streams of clustering algorithms exist:

- Partitioning methods
- Hierarchical methods.

Partitioning methods such as K-Means [31], Neural Gas [24] and Self-Organising Maps (SOMs) [43] operate by dividing the feature space into an optimum set of clusters which are represented by a set of prototypes. A limitation with many partitioning methods is their dependency on knowing the number of partitions or pattern groups n.

Hierarchical methods avoid the specification of n by producing a tree or dendrogram for all possible divisions according to some similarity metric. An appropriate level of representation can then be specified by a termination constraint, thus cutting the tree at some level.

2.3.1 Self-Organising Maps

Self-Organising Maps or SOMs, having a particular application in the colour correction method presented later, are further discussed. It has been stated that having to know the number of divisions n limits the unsupervised nature of partitioning clustering schemes. SOMs have the ability to overcome this limitation, thus making them ideal for analysing completely unknown feature spaces.

A SOM [43], which is essentially a Kohonen Neural Network, is a two-layer network where the input layer is interconnected to the output layer (as with conventional neural networks). However, the output layer (competitive layer) is also structured to form a 2-dimensional grid (shown in Figure 2.9).

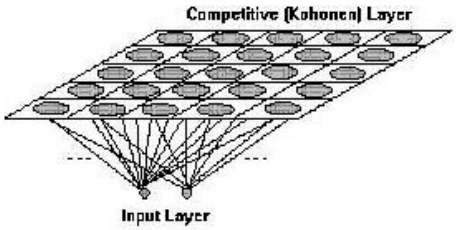

Figure 2.9: *Structure of a Self-Organising Map (SOM).*

During training, each output node is moved so as to be closer to an input vector. In addition, neighbouring output nodes are also moved towards each other according to some neighbourhood function. This has the effect of quantising the input vectors, by folding the grid of neurons around the presented data. Eventually the output grid becomes an ordered map with similar prototypes close together, thus preserving the topological structure of the feature space.

SOMs are therefore able to extract the intrinsic patterns of a feature space with their only constraint being the specified number of training prototypes, which is normally automatically estimated from the size of the feature space. Features of SOMs include simple classification (using simple nearest neighbour), dimensionality reduction and data compression. In addition, hierarchical SOM methods (eg. Growing Hierarchical SOM [8]) have shown potential in clustering of multi-scale data.

Chapter 3

Architectural Overview

The primary goal of the system is to provide a suitable framework for person/object matching that can be extended over a network of cameras. Since video processing is extremely resource-hungry, a distributed computing, bottom-up paradigm was chosen as the basis for this framework. In terms of actual processing, Figure 3.1 encapsulates the ideal functionality of the system.

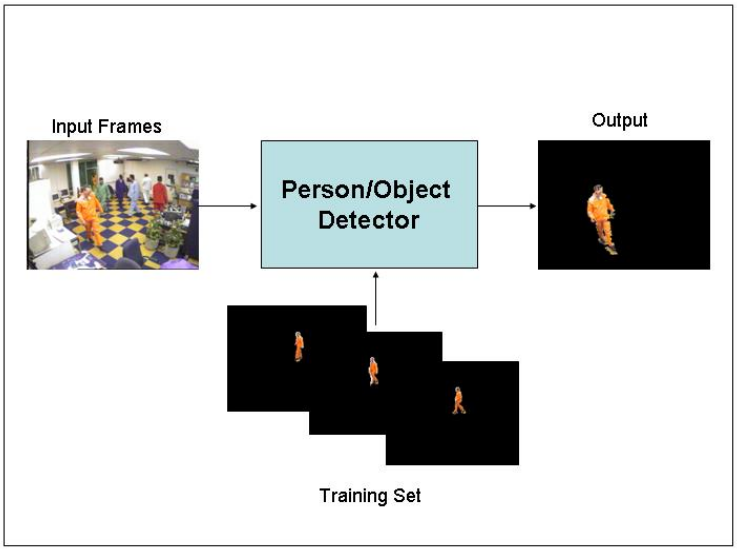

Figure 3.1: *Ideal System.*

A camera provides input frames to the Person/Object Detector (referred to subsequently as POD). Previously trained colour object models are then used in a matching process which identifies the location (if any) of the target in the input frame.

3.1 Bottom-Up versus Top-Down

Like many other systems, recognition algorithms can be approached in either a 'bottom-up' or 'top-down' methodology [40]. Bottom-up systems are data-driven. Starting from the input (bottom), subsequent data levels are built upwards by feature extraction until a level is reached where the features can be compared to the target model (top).

On the other hand, top-down processes operate in a concept-driven manner. A search over the parameterised target model (top) yields a predicted view of the target which is then compared to the actual input. The example shown in Figure 3.2 illustrates these differences.

The fundamental difference between the two methods is that while bottom-up processes build up knowledge from raw data, top-down processes predict lower measurements by assumptions of model coherence. As a result, top-down systems generally express the entire system as an optimisation problem of measuring the similarity between a predicted view (based on model parameters) and an observation. This provides a good representation of the abstraction process, however becomes inefficient when searching a high dimensional parameter space (common in person/object tracking applications) [6]. Consequently, top-down procedures usually require a wealth of prior information (eg. previous observations, kinematic constraints and camera pose information) in order to make the parameter search tractable.

Since the POD system is aimed at a fast absolute (no prior information) classification, a the bottom-up, modularised design was selected.

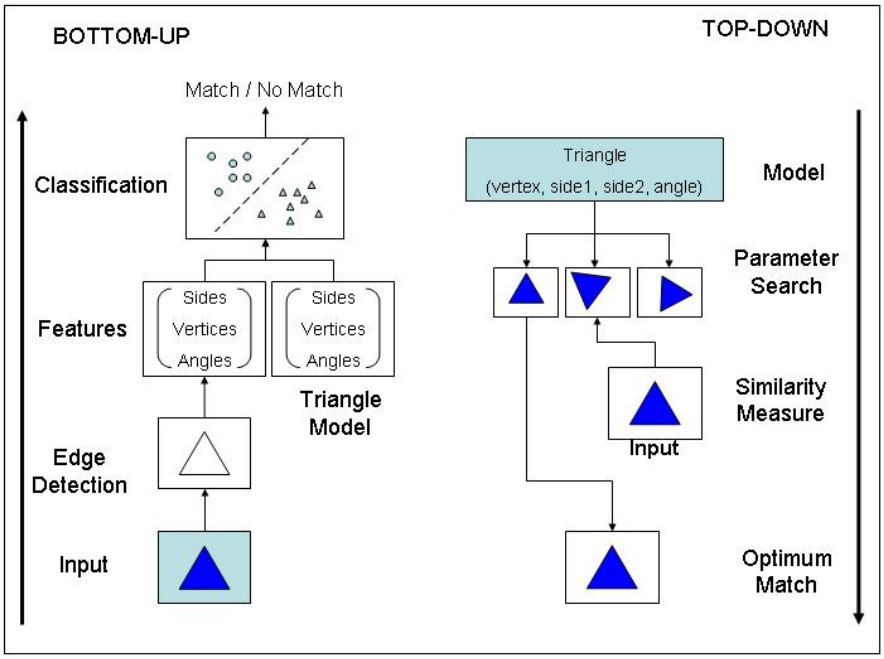

Figure 3.2: *Example of Bottom-Up vs Top-Down systems.*

3.2 Physical Layout

The nodes in the distributed framework, shown in Figure 3.3, have been defined by three primary functions: Processing; Storage; and Management. While the diagram depicts that each node be allocated its own computer, the framework is intended to be flexible so that multiple node processes can be economically run on a single machine. Naturally, this only applies if real-time operation is not a requirement (i.e. off-line analysis).

Each processing node handles one to two cameras. They are responsible for segmentation, feature extraction, matching and model updates. High-level data, produced by the processing nodes, is then synchronised with a storage node which provides global consistency between all nodes.

In terms of the Client/Server model, processing nodes act as hidden servers which

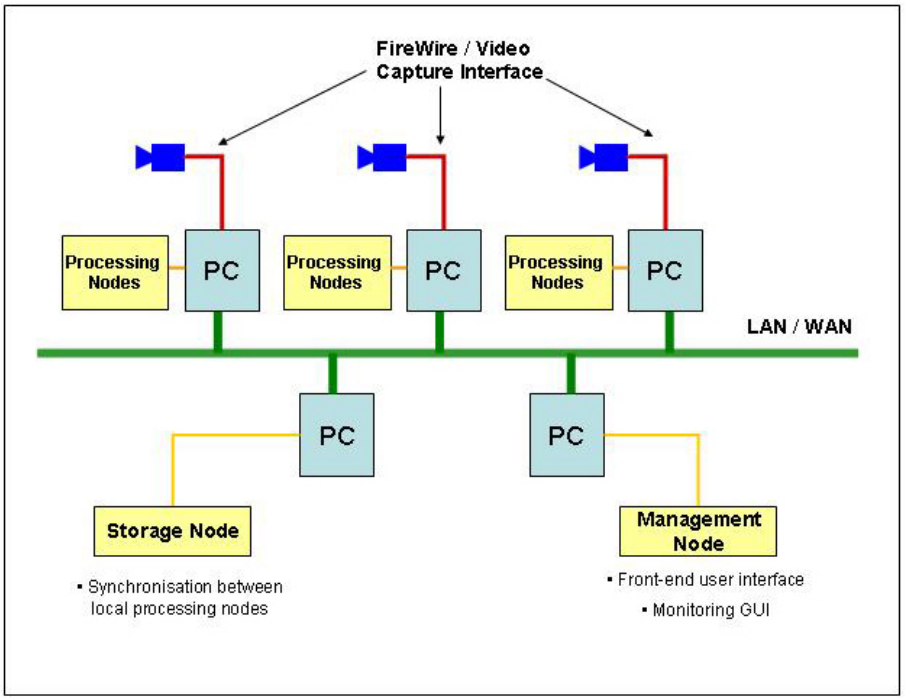

Figure 3.3: *Distributed Framework.*

serve information to a central point (i.e. storage node). Clients access the high-level image information from the storage node though a management console. Direct connections between the management console and processing nodes are also possible should a live video stream be required. Ideally operators would mainly access the high-level data streams from the storage node, thus minimising the network transmission load.

This framework therefore allows a modularised processing approach while preserving coherence between the multiple data streams.

3.3 Data Flow Model

The processing nodes discussed in the previous section encapsulate the entire functionality of the POD system. The system comprises several pre-processing steps which

feed into the matching and training processes. A local object model repository provides the stored features of current targets which are used during matching. Figure 3.4 depicts these operational stages for a single processing node.

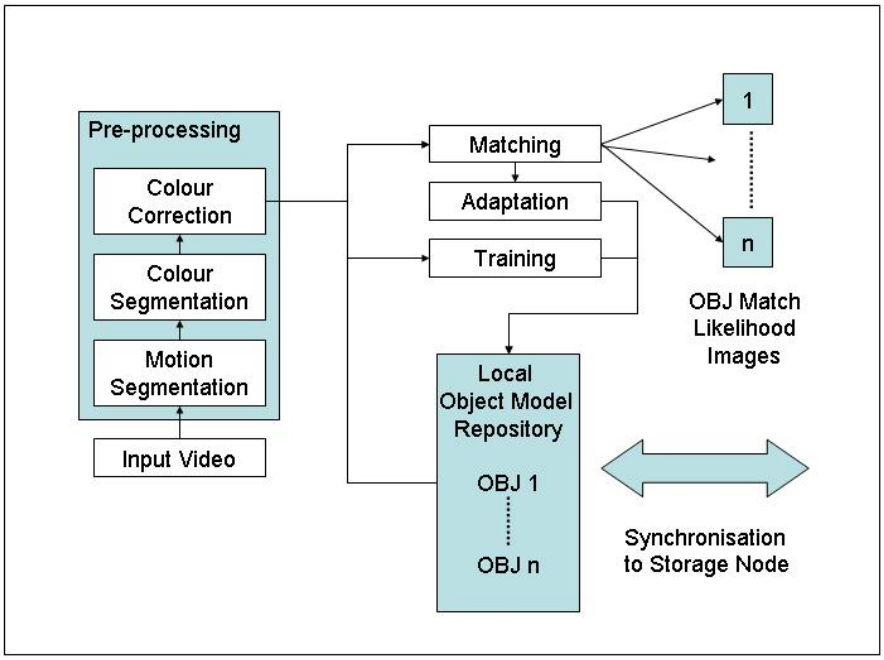

Figure 3.4: *Processing Node Data Flow Diagram.*

The first stage is the digital acquisition of video from a camera. The image is equalised and filtered for noise using histogram analysis and median filtering respectively.

Following this, three pre-processing steps are used to extract colour features: Motion Segmentation; Colour Segmentation; and Colour Correction. In order for the matching process to be as fast and effective as possible, it should be presented with as little irrelevant data as possible. This allows the sensitivity threshold to be increased without resulting in excess false positive matches. Searching less of the image relates directly to a faster matching process.

Motion segmentation is used to separate active people and objects from the static background thus reducing the clutter by a significant amount. Colour segmentation

then groups similar pixel regions, together thus producing a compressed representation of the motion segmentation. This allows concise models to be constructed and greatly reduces the computational cost of matching.

When viewing an object with different cameras, it is unlikely that it will appear identical. Factors such as camera gain, shutter speed and gamma correction can contribute to large variances in image formation. Additionally, since each camera will most likely be positioned differently (probably in different rooms), environmental lighting conditions will also cause inconsistency between views. Since the system must be able to compare a person or object's colour between views, a method of calibrating all cameras to a common colour subspace is necessary. Towards this end, the colour correction stage uses trained samples of a camera's response to a range of colours in order to calculate an appropriate adjustment.

The features produced by the pre-processing stages are represented by a cluster of colour centres. They are then applied to the core of the system. Initially, since the object model repository will be empty, the training stage will use the features of a specific target to discover the best representation for that target. This trained feature set is then added to the object model repository.

Once trained object models are available, the matching process is activated and produces a likelihood response to the existence of each target listed in the local repository. Close matches are processed through an adaptation stage and used to incrementally update the stored models. This allows the system to track gradual drifts caused by lighting artifacts. Information about each matched target is compiled into a running profile and stored. Finally, the likelihood outputs can be combined, and together with the input image produce a labelled image of the position of any visible targets.

The next four chapters provide a break-down of each processing stage.

Chapter 4

Segmentation

Segmentation is the process of extracting relevant information from an input data stream for a specific application. In visual tracking, segmentation normally refers to automatically separating a desired object or person from a background scene. While ideally the segmented foreground image should contain all the pixels relevant to its target, in reality this entity is extremely difficult to define.

In the POD system, segmentation is a pre-processing step thus requiring it to be optimised for speed. A simple two-part segmentation scheme is used for reducing clutter and extracting colour features from objects. Firstly, *motion segmentation* by way of background subtraction removes target candidates from the static background scene. The next step involves a *colour segmentation* process whereby regions of similar colour in the foreground are grouped together and represented by a cluster of colour centres. This reduces the load on the training and matching stages, and provides a concise object description system capable of being synchronised over a network.

4.1 Motion Segmentation

Owing to the fact that model training focuses only on significantly large and consistent colour regions of the foreground object, exact segmentation was not a priority.

Therefore a simple adaptive background subtraction algorithm was used.

4.1.1 Background Subtraction

Essentially, background subtraction operates by taking a frame BG containing only the static background, and subtracting a consecutive frame P from it. Any pixel difference which deviates more than a set threshold T_{diff} is considered foreground (shown in Equation 4.1). In this way a foreground mask M can be obtained:

$$M_{(x,y)} = \begin{cases} 1 & if\ |P_{(x,y)} - BG_{(x,y)}| > T_{diff} \\ 0 & otherwise \end{cases} \tag{4.1}$$

In reality, thresholding all pixels in the image by the same amount does not provide reliable results, as demonstrated in Figure 4.1.

Figure 4.1: *Segmentation using thresholded background subtraction.*

Factors such as light distribution and colour differences can cause inconsistencies in the comparison between foreground and background pixels. Additionally, it is unlikely that the background will remain entirely static due to persons interacting with furniture and objects. Also, shadows cast by foreground objects may cause background to be regarded as foreground. Therefore, realising a segmentor that can cope with such problems led to two useful strategies:

1. Adaptive Pixel Modelling
2. Shadow Removal.

4.1.2 Adaptive Pixel Modelling

An alternative to using a global threshold for the subtraction is to assume that each pixel deviates according to its own model, and thus to threshold each pixel in the context of its model [41]. For simplicity and speed, a unimodal normal distribution was used here.

If each pixel is assumed to vary with a normal distribution over time, then it can be represented by a mean $\mu_{(x,y)}$ and a variance $\sigma^2_{(x,y)}$ (assuming a single channel, grayscale image). A background model BG can then be adaptively updated from consecutive input frames P as suggested by [25]:

$$\mu_{BG_{(x,y)}}(t+1) = (1-\alpha)\mu_{BG_{(x,y)}}(t) + (\alpha)\mu_{P_{(x,y)}}(t+1) \quad (4.2)$$

$$\sigma^2_{BG_{(x,y)}}(t+1) = (1-\alpha)\sigma^2_{BG_{(x,y)}}(t) + (\alpha)\sigma^2_{P_{(x,y)}}(t+1), \quad (4.3)$$

where $(0 \leq \alpha \leq 1)$ and controls the rate of adaptation. Typically, a high value for α is used to initialise the model after which the value is lowered so that the model does not adapt to foreground motion. An α of approximately 0.05 was found to provide a good balance, allowing the system to cope with slow, variations in lighting. Although small, repetitive motion of small regions can produce jitter which does not conform to the unimodal normal distribution [35] (eg. leaves swaying in wind), these areas are usually small and isolated and can be filtered out by morphological processing.

Each pixel in the input frame P is then assumed to be part of the foreground mask M if it meets the condition:

$$|P_{(x,y)} - \mu_{BG_{(x,y)}}| > \max(k\sigma_{BG_{(x,y)}}, n_{CCD}). \quad (4.4)$$

The constant k determines the threshold and is typically 3 while n_{CCD}, representing the camera's internal CCD noise, ensures that σ^2 does not become too close to zero.

This procedure can then be applied to colour images by simply modelling and adapting each colour channel's mean and variance separately (i.e. $\mu_{R(x,y)}$, $\mu_{G(x,y)}$, $\mu_{B(x,y)}$ and $\sigma^2_{R(x,y)}$, $\sigma^2_{G(x,y)}$, $\sigma^2_{B(x,y)}$).

4.1.3 Shadow Removal

The second artifact which can cause inaccurate segmentation is the interaction of shadows. When a moving person or object casts a shadow over the background model, the covered pixels become darker and can exceed the adaptive threshold thus causing them to be incorrectly associated with the foreground.

Approaches to shadow reduction range from approximation using models to adaptive thresholding and chromatic analysis. A popular method is to notice that shadows cause a reduction of lightness over the covered region without affecting the chromaticity (hue and saturation) [25]. Therefore, certain shadows can be removed by modelling the background in chromaticity co-ordinates such as CIE xy, rgG, etc[1]. Unfortunately, while in practice this removes shadows, discarding the luminance information can lead to instability [21] since any true foreground areas whose chromaticity matches the corresponding background model will be erroneously classified as shadow (eg. a green shirt in front of grass).

A compromise is reached by using first-order gradient information to detect shadows with soft edges as proposed by [25]. When an object has similar chromaticity to its background, its gradient image will differ depending on the textural differences between the two. Therefore the foreground is detected by the differential change of either the chromaticity or gradient models. One downfall is that the method is can only deal with soft-edged shadows (which are common). Strong shadow edges (areas of large contrast) will produce a large gradient differential and therefore be incorrectly labelled as foreground. The gradient model, as stipulated by [25], comprises of three gradient means (μ_{xr}, μ_{yr}), (μ_{xg}, μ_{yg}), (μ_{xb}, μ_{yb}) (one for each RGB channel)

[1] Colour spaces are discussed in Section 2.2.3.

and corresponding magnitude variances σ^2_{gr}, σ^2_{gg}, σ^2_{gb}. Gradients are constructed by convolving each image channel with the Sobel X and Y operators. Pixels are then adapted and thresholded in exactly the same manner as discussed in the previous section (see Equations 4.2 and 4.4).

In order to improve the process, CIE L*a*b* co-ordinates are used in place of RGB (on account of their better pixel differences). Further, by only creating gradient models for the L* (intensity) channel, the nine parameters (originally six RGB gradient means and three variances) are reduced to three, i.e. (μ_{xL*}, μ_{yL*}) and σ^2_{gL*} (gradient mean requires two parameters — x and y components). Although this reduces the sensitivity of the gradient measure between different colours, it provides a manageable model that can operate close to real-time and therefore not hinder system performance.

4.1.4 Implementation

The combination of the modelling and shadow removal forms a robust basis for the motion segmentor. The final background pixel model is a function of six parameters, $BG_{x,y}(\mu_{a*}, \mu_{b*}, \mu_{xL*}, \mu_{yL*}, \sigma^2_{a*b*}, \sigma^2_{gL*})$, where co-ordinates are described in the CIELAB colour space and the chromaticity variance is calculated as the magnitude of the difference in the a*-b* plane. A foreground mask is thus extracted from an input frame via the process shown in Figure 4.2.

After converting to CIELAB, x and y first-order Sobel gradients are constructed. The sum of the squared difference between the gradient images and their corresponding model means (μ_{xL*}, μ_{xL*}) is then calculated and compared with the gradient magnitude variance model (σ^2_{gL*}). Similarly, a chromaticity magnitude image is calculated and compared with the chromaticity variance model (σ^2_{a*b*}). An initial foreground mask is thus constructed by combining the two results.

The intermediatory foreground mask now consists of large foreground objects and many small uncertainties. Assuming that true foreground objects (eg. people) will

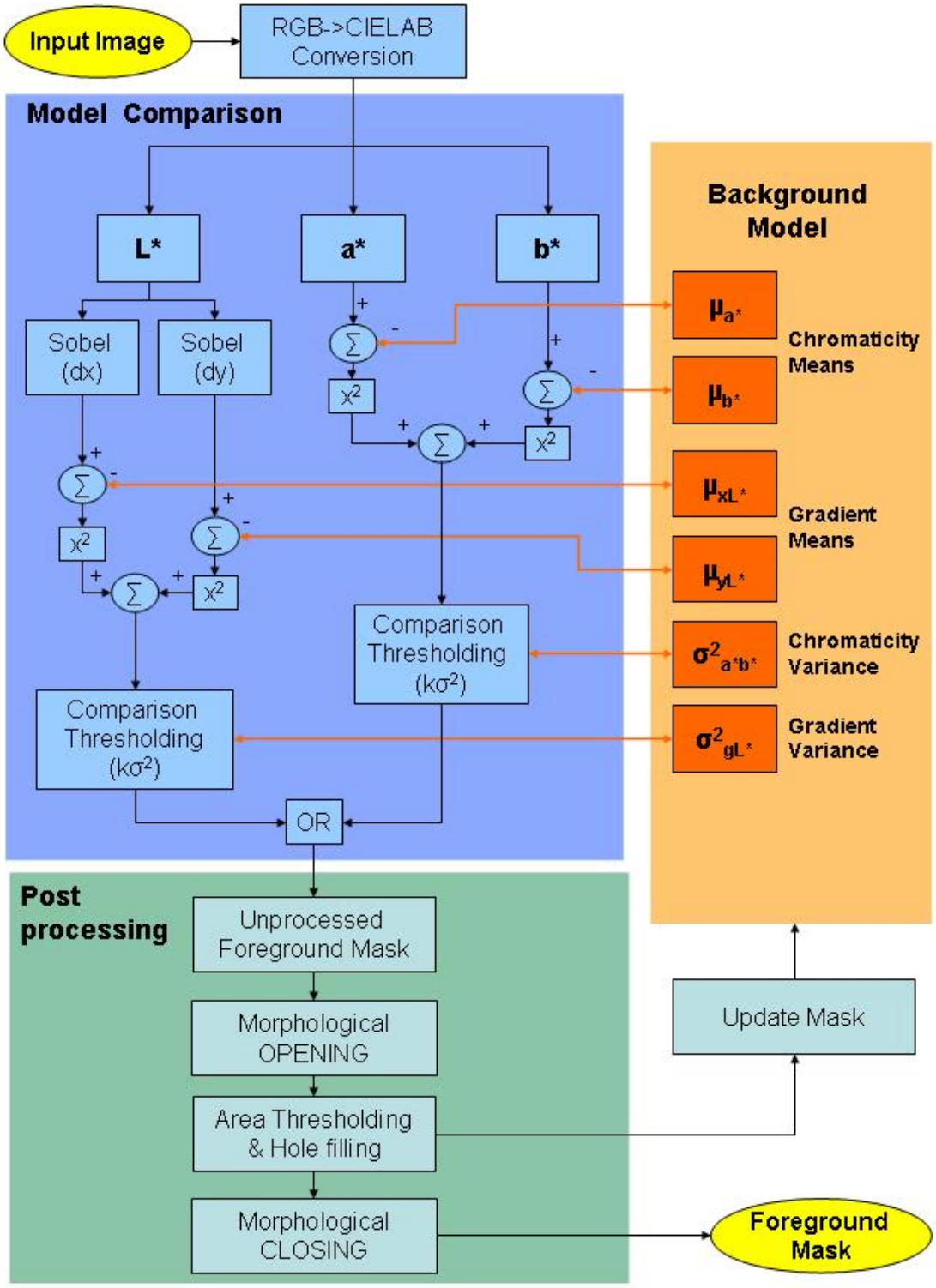

Figure 4.2: *Motion segmentation flow diagram.*

occupy a minimum blob (connected component) area, morphological opening is used to remove isolated pixel noise. This is followed by a minimum area thresholding procedure which also fills in isolated holes inside object masks should they be less than a filling area threshold. The area thresholding process also constructs an update mask used to determine which areas of the image should not be included in updating the background model (i.e. any probable foreground). Once completed, a morphological closing ensures that object edges are restored from the original opening function. Since the small, noisy areas have already been filtered out, only the remaining foreground objects are affected. The end result is a binary foreground mask which identifies any significant motion. An example of the result is shown in Figure 4.3.

Figure 4.3: *Adaptive Background Segmentation with shadow removal.*

4.1.5 Limitations

Background subtraction is limited to use with static, fixed cameras due to the nature of the subtraction (so that the background image stays the same). The process also requires that the initial model be trained without any potential foreground objects — otherwise the background model would learn these.

The fact that the POD system uses the segmentation simply as a load reducing filter allows these limitations to be less restrictive. Firstly, moving the camera will

simply produce more foreground regions which need to be searched. The initial-training limitation can also be overcome by adding the matched objects of a first unsegmented frame to the update mask, thereby stopping the initial adaptation from including these objects in the background model. This obviously implies that the object models are known beforehand and therefore the initial object modelling process must use images from a static camera.

4.2 Colour Segmentation

A typical 352×288 image contains over 100 000 pixels. Since it is desired to train models relating to distinguishable coloured areas of an object, it would make sense not to have to process every pixel in order to determine its colour grouping. Therefore a batch colour segmentation method allows an efficient quantisation of the foreground into coloured components, leading to a more compressed data representation which is better suited to higher-level processing. As colour segmentation applies to the training of object colour models, the process operates on the segmented foreground mask produced by motion segmentation.

Region-based segmentation has been a particular interest in image content-based retrieval databases where, a huge number of images must be searched for feature matches. The compact nature of segmented images allows for more generalised and faster searching. In contrast to the motion segmentation process, region-based methods are normally localised to the similarity of regions within a single image. Some techniques which are conventionally applied to the problem include: optimised amplitude thresholding [31]; recursive region growing [1]; K-Means clustering [31]; and vector field analysis [42].

Preliminary comparative testing performed by [23] towards the goal of fast, automated segmentation showed that multiscale processing methods are the most appropriate when speed optimisation is a requirement. This confirmed our findings that the use of pyramid segmentation by way Gaussian pyramid decomposition was an efficient

mechanism for the colour segmentation process.

4.2.1 Pyramid segmentation

Multiscale image processing techniques are hierarchical processes which use multiple resolutions of an image to perform analysis. These can be approached as top-down (quad-tree decomposition) or bottom-up processes (image pyramids). In the latter methods, image levels are constructed by downsampling the image by a series of filters — Gaussian in this case — which provides a smoother output.

The OpenCV library [18] provides a well optimised implementation based on the algorithm proposed in [6]. The input image (largest) can be thought of as the base of the pyramid. Each consecutive level is then built upwards, downsampling by a factor of two at each stage, until a specified maximum level is reached (commonly between 3 and 5). Two thresholds, T_1 and T_2, determine the nature of the segmentation, and linking is performed in two stages illustrated in Figure 4.4.

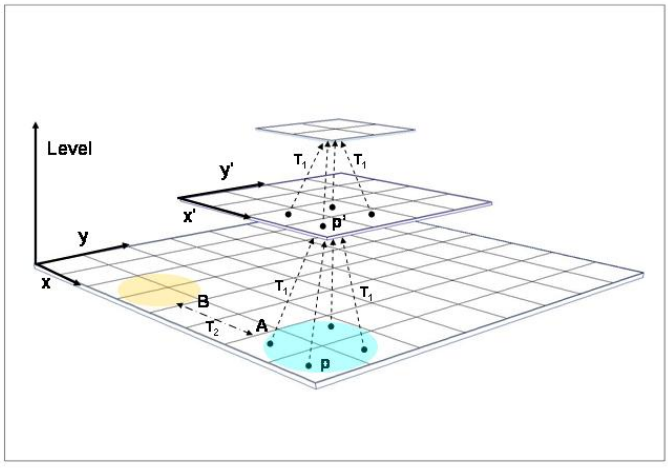

Figure 4.4: *Pyramid segmentation process.*

1. A link between a pixel $p_{x,y}$ on level L and its candidate father $p'_{x',y'}$ on level

$L+1$ is established if: $\text{dist}(c(p_{x,y}, L), c(p'_{x',y'}, L+1)) \leq T_1$.

2. Connected components A and B are then clustered together if: $\text{dist}(c(A), c(B)) \leq T_2$.

The function *dist* is the Euclidean distance between local property functions c for each pixel. The local property c is the type of measurement associated with a pixel, which in this case c is simply the intensity of the pixel. Therefore, the distance calculated by the *dist* function is effectively the difference in pixel intensities $|i(x,y) - i(x',y')|$. For colour images, the intensity is calculated by the weighted grayscale approximation:

$$\begin{aligned} |i_{RGB}(x,y) - i_{RGB}(x',y')| &= 0.30|i_R(x,y) - i_R(x',y')| + \\ &\quad 0.59|i_G(x,y) - i_G(x',y')| + \\ &\quad 0.11|i_B(x,y) - i_B(x',y')|. \end{aligned} \tag{4.5}$$

4.2.2 Implementation

As previously mentioned, the pyramid segmentation scheme from the Intel OpenCV library was used for the system's colour segmentation. The fact that this method produces connected components which are not necessarily spatially linked (global clustering) led to a minor post-processing modification. This involves scanning through the list of presented regions and splitting unconnected components having the same label into a separate region. Further, a lower-bound area threshold (10 pixels) was set in order to stop noisy one- and two-pixel regions from being submitted as features.

Parameter tuning, which is the thrust of [23], was found to be fairly inconsequential. Unlike [23], the primary goal was to reduce the mass of pixel data to a manageable number of classes (approximately 5% of the image pixels). Therefore exact parameters for maximising the quantisation was not required. In fact, a larger list of small regions which more accurately describe the original pixel colours is preferred. In general, setting $T_1 = 30$ and $T_2 = 10$ provided equitable results. Figure 4.5 shows an example output.

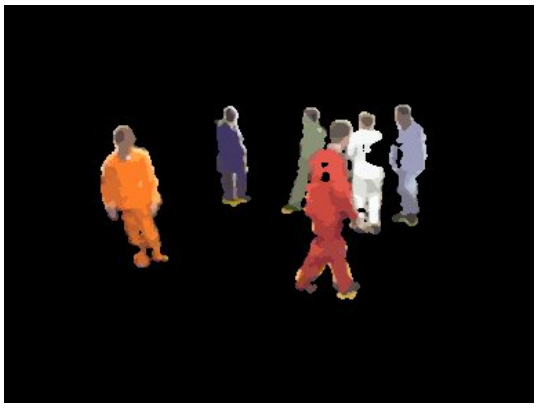

Figure 4.5: *Example of applying pyramid segmentation.*

4.2.3 Limitations

The only inherent limitation of the pyramid segmentation method is its tendency to merge unrelated colours if the thresholds are set too high. Since the POD system does not require an optimised minimum set of clusters, fixing the thresholds at the previously suggested values ensures that high definition separation is maintained.

One other minor artifact involves the size of the input image. Since downsampling requires image dimensions which are divisible by two, the input image must be padded so that it can be downscaled a number of times.

Chapter 5

Colour Correction

One of the primary requirements of a multi-camera colour tracking system is consistency of colour measurements between several cameras. Colour constancy refers to the correction of colour deviations caused by a difference in illumination [47]. Failure of the system to provide a correlation between similar colours over the camera network would cause colour-based appearance models to become invalid once a person leaves the view of any camera. Figure 5.1 shows an example of two unmatched surveillance cameras.

Figure 5.1: *Example of mismatched cameras (Images from VS-PETS 2001)*

5.1 Colour constancy approaches

The problem of colour constancy has been under scrutiny for some time in the image retrieval area, where the classification of images is sometimes reliant on the similarity of colours. The general trend is to find an illumination invariant transform from the usual RGB pixel representation, which provides consistent measurements irrespective of the illumination direction, surface orientation and intensity. Examples of such transforms include normalised RGB (rg) and HS (Hue-Saturation), which provide good colour invariants under white light [3]. However, in a real camera environment, lighting configurations will cause different camera hardware to measure different hues (device dependent colour spaces), thereby invalidating any such invariant. This means that before such information is to be of any use, the dynamic ranges of the contrasting images must be normalised. Methods for achieving colour constancy generally fall into one of three groups:

Physical Modelling: These methods involve formulating an invariant by analytical derivation of spectral image formation from its physical processes. Since lighting models are extremely complex, many assumptions and generalisations are made about the scene in order to isolate the primary processes. An example is the work presented by Geusebroek et al. in [16], which deals with finding a colour invariant for scenes in which the illumination colour changes over time.

Human Vision Modelling: Here processes are modelled after the human visual system, which tries to maximise image dynamics while perceptually normalising the scene information. Several illumination adaptive mechanisms, which are attributed to low-level eye functions, have been explored in image processing. One such mechanism is the hypothetical *White Patch* reference. This normalises the colour channels towards an ideal white point reference. Another mechanism, known as *Gray World*, involves adapting the image dynamics so that they fall within a comparable range. This relates directly to matching image dynamics by performing a type of mean-level adjustment. A combination of such mechanisms, as in [33] and [32], has proved viable towards performing unsupervised

colour correction.

Model Normalisation: By assuming a generalised lighting model (eg. Lambertian or Specular Reflection), the entire illumination process can be broken into a series of transforms. Unwanted components can therefore be removed (by making certain assumptions) and thus result in an invariant set of colour co-ordinates. While this seems similar to the *Physical Modelling* methods, the difference lies in the assumptions, which use models of human visual responses and not exact physical processes. These methods therefore bridge the previous two groups. An example is the work of Finlayson and Xu [12], which uses the log RGB space for colour normalisation. They derive pixel colour using a Lambertian lighting model and scale the channel means using Gray World normalisation. The benefit of using log RGB space is that *products* become *sums* and therefore removal of components can be achieved by a simple subtraction. Most importantly though, device gamma (which is a power function) can be cancelled out using logs. This is extremely useful when comparing images from different cameras.

5.2 Unsupervised colour correction using SOMs

In light of the fact that our system is geared towards near real-time operation, it follows that a fast, robust colour constancy method is needed. Since we are using multiple cameras, the method must be insensitive to camera pose and position in addition to the usual invariants. The Video-CRM system described in [17], which has similar requirements, proposes the use of a colour calibration target. The basic idea is to show the calibration target to each camera and use the responses to calculate the gamut mapping between the two image systems.

In a large camera network, however, it is desirable to have a more automated approach which does not encumber the users. In any case, mapping based on a target can never be totally accurate unless it takes into account colour or intensity shifts within a single image frame. This would require the calibration target to be evaluated at

several positions for each view, leading to a lengthy calibration procedure.

Austermeier et al. [2] have shown a useful method for performing an unsupervised, target-based calibration scheme for normalising illumination changes. Their tests showed that a cloud of RGB pixels (plotted by omitting their spatial image placement) preserves its topology when subjected to a change in illumination. Furthermore, if the clouds of the original and resulting images are each quantised by a set of SOM prototypes[1], pixel colour can be corrected by simply translating its prototype between the two maps. SOMs have the useful feature of being able to quantise data into a set of prototypes, while at the same time preserving topological relationships between neighbouring neurons.

To clarify, usually the main usage of SOMs is for dimension reduction of feature data. However, in this application it is simply used as a 3-D data-fitting method. Another common practice is to use a 2-D neuron grid for the SOM. The main reason is because its distance matrix (depicting clustering information) is best understood in planar form. Once again, since this scheme is using the SOM's fitting ability, it is necessary to use an exact representation of the data, and thus the map is created as a 3-D lattice.

As an example, consider the two camera views presented previously in Figure 5.1. Figure 5.2 shows a plot of RGB clouds for each image. As expected, the brighter left-hand side image (red crosses) has a greater dynamic range, indicated by the larger RGB values.

If the clouds are now quantised into two 3-D SOMs, the original pixels can now be represented as a reduced set of prototypes (Figure 5.3). The most important factor is that each SOM must be identically, linearly initialised before being adapted to a data cloud. This creates an intrinsic mapping link between corresponding prototypes and allows inter-SOM mapping by simply calculating translation vectors for each prototype. Using this idea — namely that neighbourhoods of pixels can be mapped to a reference — all that is required is a set of translation vectors defined for each

[1]SOMs are reviewed in Section 2.3.1 and the training procedure is outlined in Appendix A.

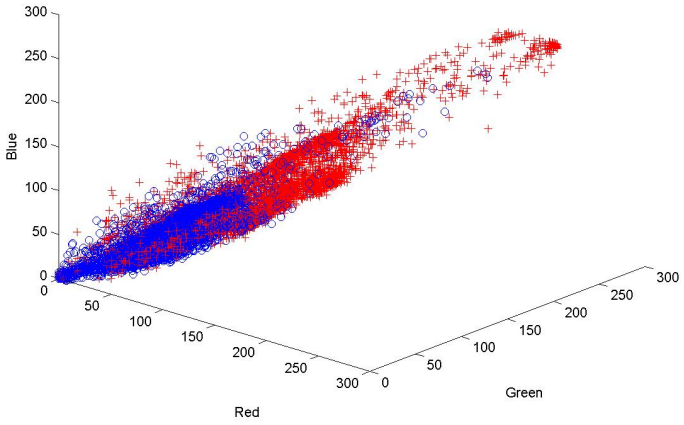

Figure 5.2: *RGB clouds for images in Figure 5.1. Red crosses and blue circles represent the original left- and right-hand side images respectively.*

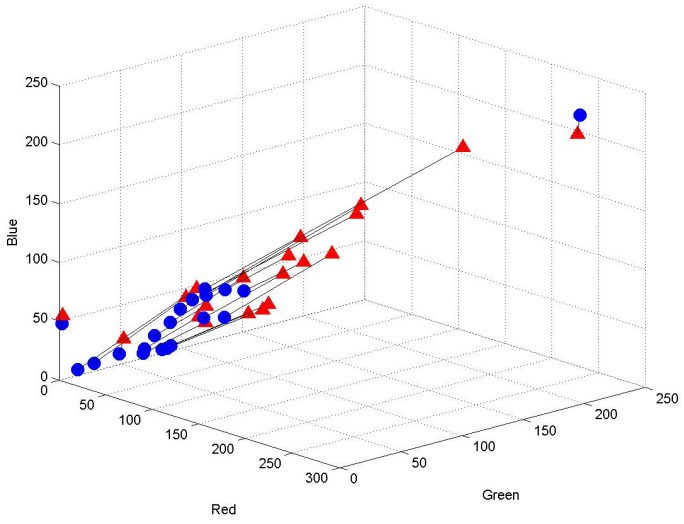

Figure 5.3: *SOM prototypes for each RGB cloud shown in Figure 5.2. Red triangles and blue circles represent the red cross and blue circle classes from Figure 5.2. Black lines show the translation vectors between each map.*

neighbourhood. These are indicated by the black connecting lines in Figure 5.3.

As seen in the above figure, the SOM not only compresses the data representation, but also provides the translational relationships between pixel neighbourhoods between images. Therefore, once the pixels in the darker image (blue class) are translated by the SOM vectors (black lines), image balance is improved. The result of correcting the second image with respect to the first image is shown in Figure 5.4. Owing to the quantisation process the output image lacks smoothness. However, if the CIELAB co-ordinates of similar surfaces are compared between the unmatched views (eg. the grass and road areas), it is found that colours in the corrected image are on average two times closer than the uncorrected image (using CIELAB distances).

Figure 5.4: *Images before and after SOM processing (top and bottom rows respectively)*

5.3 Implementation

The colour correction process in the system flow diagram in Figure 3.4 (Chapter 3) is shown to follow the colour segmentation stage. This is because correcting fewer pixels is faster, and because only the segmented targets need to be corrected in order for model colour matching to succeed. Training of the colour correction mappings, however, operates directly on the input images.

There are some problems with the SOM method proposed by [2]. Firstly, they recommend training the image pixels using a $25 \times 25 \times 25$ SOM grid. SOM training time tends to follow an exponential trend as the map size increases. Additionally, the size of the set of input data also contributes to the number of training steps and amount of memory required.

Since it was not tractable to follow the suggested parameters, it was decided to pre-quantise the pixel data into similar classes in order to reduce the amount of data being presented to the SOM. The natural choice was to use the existing pyramid segmentation[2] scheme which retains the major colour groups. While this reduced the computation significantly, memory resources still restricted the map size to a level that could not adequately represent the data.

The second modification was therefore to split the input data into several batches and to train a small SOM ($5 \times 5 \times 5$) for each batch. Once complete, all the SOM prototypes could be recombined and used per normal. For the splitting process to work, it was important to retain coherence between each image's prototypes so that the SOM's topological information would remain intact. Thus, in place of training a SOM for each image part, a single SOM was trained to the first input and then adapted to the second. Finally, it was found that using CIELAB co-ordinates in place of RGB provided better results, since CIELAB space produces a smaller distance error[3] when quantising colour values.

[2] Details given in Section 4.2.

[3] Intrinsically, colour perception in CIELAB is supposed to be directly proportional to Euclidean distance.

The type of correction warranted by the POD system generally requires that the general image trends be the same for a comparison. In order to provide a smoother overall response for correction, a linear least squares fit of the input-output prototype map is used as a post-processing step. The colour correction coefficients are calculated in the RGB space resulting in a fast mapping between camera views. Equation 5.1 shows the correction from pixel R, G, B to R', G', B':

$$\begin{pmatrix} R' \\ G' \\ B' \\ 1 \end{pmatrix} = \begin{pmatrix} x_R & 0 & 0 & x_R^0 \\ 0 & x_G & 0 & x_G^0 \\ 0 & 0 & x_B & x_B^0 \\ 0 & 0 & 0 & 1 \end{pmatrix} \begin{pmatrix} R \\ G \\ B \\ 1 \end{pmatrix} \tag{5.1}$$

The result of the final implementation is shown in Figure 5.5 using the same images from the previous example. The smoother response in the corrected image is evident and the perceptual colour difference between the unmatched views (using CIELAB distances) is now nearly three times closer for the corrected image.

Figure 5.5: *Camera view comparison after final processing with polynomial smoothing. Second image has been modified to match first image*

5.4 Limitations

A fundamental difference between the application of colour constancy in our system, as opposed to other contemporary work, is that we try to normalise the colour system between two different camera systems. Most results of colour constancy algorithms use computer-generated scenes as their basis for trials. While this proves that the algorithm can correct for artifacts matching the models used to create the scene, it rarely relates to the unpredictable nature of real camera views. Keeping this and the requirements of our system in mind, the colour correction implementation developed was tailored to improving the comparison of CIELAB colours between camera views, and not providing an ideal transformation.

A common problem is caused by extremely bright or excessively dark regions. Though the camera provides a non-linear output voltage from the CCD, the camera response is still limited to its range (dictated by the aperture setting, shutter speed and gain). Therefore without being able to dynamically modify camera parameters, a digital image processing system cannot recover information which has fallen outside the range. Simply put, if the image values saturate at either 0 or 255 (RGB sensor limits), it is generally not possible to determine the true colour of the pixel. In colour constancy, this means that for two different camera views, there are only two possible adjustments:

1. Normalising the dynamic range
2. Adjusting data within the dynamic range of the image.

The unsupervised nature of the method relies on the fact that similar, but distorted, colour classes exist in both images. Therefore the system is limited to correcting scenes which have similar environmental colours. Should varying environments need to be matched, a calibration target or known object must be present in each scene in order to determine the general difference. This could be achieved by having a person wearing a suitably coloured jacket traverse the various camera areas. All failing, a

final alternative is for the system to ask a user to manually specify matching colours between scenes using a pixel selection tool.

Chapter 6

Object Modelling and Training

At first, it was hoped that a full unsupervised training method would be achievable by the analysis and filtering of the segmented images. The original idea was to determine the presence of a single person or object from the segmented mask by observing the tendencies of certain colours to move together on average.

Ultimately, it was decided that this process could best be implemented in the future, after a solid matching process (the primary objective of the thesis) was established. This resulted in a semi-supervised training process which self-determines the 'best' colour features corresponding to a target, given the set of features from several images of that target.

6.1 Design Aspects

What makes an object visually distinguishable from its background? Commonly, this tends to be a combination of: geometric shape and size; texture and colour; and prior knowledge about its environmental likelihoods (for instance, trees tend to be situated

outside).

In particular, humans make extensive use of colour in recognition. This is probably due to the virtually instantaneous nature of colour information. For instance, someone describing a car would normally note its colour before its make or model. This means that once a target has been identified, short-term (and sometimes long-term) tracking can be maintained by colour matching. Of course this process does rely on the fact that the target's colour appearance is suitably distinguishable from its background.

With regards to the POD system, the aim was for training to accept input samples from either a user-selected area or a motion-segmented data stream (controlled by the matching process). Since training samples for an online system are sparse, it was further decided to design a modelling process which can create a reasonable object representation based on a single observation. Additional observations are then used to refine the model. The result is a training method which operates by filtering the segmented colour features based on the following criteria:

- Which colours are chromatically most distinctive?
- What are the general proportions of each colour?
- On average, which colours are most visible?
- How well is each colour matched between training steps?

Most of the time, colour is an extremely meaningful descriptor of an object, eg. blue sky, pink skin, brown hair. Other times, it can provide incorrect or no information at all, eg. dark areas, oddly lit environments. The fact that colour is not totally infallible suggests that machine vision trackers should, like humans, employ a variety of different types of features.

There are three main reasons why other visual features were not incorporated into this project. The first was based on a desire to find the limitations of using colour in a machine vision system. Colour comparisons in digital imaging have proved extremely

challenging due to camera and capture hardware limitations and variations. Secondly, the system was designed with the intention of working in conjunction with other estimation techniques. This implied that focus should be centred on the neglected areas of those systems and thereby a combined system would be able to exploit the strengths of both processes. Finally, since the project tackles the problem from a feature classification standpoint, the framework easily allows for future incorporation of additional features with little modification.

A common problem with training methods is their tendency to focus on the process of creating a descriptive model of the data and ignoring its accessibility to the matching process. This means that while analysis of each trained model provides a good high-level representation of that object, comparisons between object models are limited by the efficiency of the matching process and its associated distance metrics.

An example of this is an object which is modelled by several histograms. While the histograms may encapsulate the object's tendencies, it does not account for the fact that many histogram comparison methods do not provide consistently reliable results. Additionally, the presence of multiple object models would require an exhaustive search thereby impeding the hope of a near real-time system.

The development of the POD training process was therefore preceded by design of an efficient matching process. This was then followed by an analysis of how matching could be improved by affecting the training process.

6.2 Colour Features

A primary assumption upon which the system is based is the notion that a qualitative measure for the difference between colours exists. The CIELAB colour space provides such a measure by providing uniform colour co-ordinates which describe perceptual colour differences using the magnitude of the Euclidean distance between two points[1].

[1]Details given in Section 2.2.3.

The training procedure therefore begins by converting the RGB feature list presented by the colour segmentation[2] to their CIE L*a*b* counterparts. The system's main feature vector is therefore simply:

$$\mathbf{F}_n = (L*_n, a*_n, b*_n), \tag{6.1}$$

where $\mathbf{F}_n$ is an arbitrary feature vector. Training is split into two phases. The first is geared towards finding clusters spatially within the feature space of a presented observation set. The second clusters these cluster groups over time as additional observations are presented. The time-clustering phase therefore depends on being able to match features between observations. This is accomplished by calculating the vector of probabilities $\mathbf{P}(\mathbf{F}_n|\mathbf{C})$ of a feature $\mathbf{F}_n$ belonging to the set of centres $\mathbf{C}$ as follows:

$$d^2_{\mathbf{F}_n\mathbf{C}_i} = (L*_n - L*_i)^2 + (a*_n - a*_i)^2 + (b*_n - b*_i)^2 \tag{6.2}$$

$$K_{\mathbf{F}_n\mathbf{C}_i} = \frac{1}{\sqrt{2\pi\sigma^2_{train}}} e^{\left(\frac{-d^2_{\mathbf{F}_n\mathbf{C}_i}}{2\sigma^2_{train}}\right)} \tag{6.3}$$

$$\mathbf{P}(\mathbf{F}_n|\mathbf{C}) = \frac{\mathbf{K}_{\mathbf{F}_n\mathbf{C}}}{\sum_{j=1}^{m} K_{\mathbf{F}_n\mathbf{C}_j}}. \tag{6.4}$$

This is simply a vector formed by concatenation of the spherical Gaussian kernel activations $K_{\mathbf{F}_n\mathbf{C}_i}$, further normalised by the sum of activations of all current centres $\mathbf{C}_1 \ldots \mathbf{C}_m$. Since CIELAB offers uniformity, it follows that σ_{train} should be set to a constant value so that perceptual colour differences remain the same between classes. A $\sigma_{train} \approx 5$ has been found to provide good separation between colour classes.

Since similar colours will cluster uniformly in the feature space (due to the intrinsic nature of the CIELAB space), groups of like features can therefore be represented by a Gaussian centre. Training thus involves finding the best possible group of centres which accurately quantises the input training set — i.e. a Gaussian Mixture Model or GMM.

[2]See Section 4.2.

6.3 Gaussian Mixture Modelling

Gaussian Mixture Models have proved to be an invaluable modelling tool for estimating a data distribution. Their primary advantage is the ability to quantise data sets in which clustering is evident, thereby allowing a compact data representation. While a single Gaussian distribution cannot accurately capture the distribution of an unknown data set, an additive mixture of several Gaussian kernels can provide a much better approximation.

6.3.1 GMMs versus Histograms

Another popular alternative to GMM modelling is to use histograms. Histograms have the advantage of being adaptable to any distribution. However, there is a tradeoff between smoothness and consistency of comparisons. Secondly, where GMMs are dependent on the number of centres chosen, histogram quantisation errors arise from the selection of the bin size.

Both GMMs and histograms handle online adaptation [26], have been applied to colour appearance modelling, and produce similar results. Generally, GMMs tend to be more appropriate for smaller data sets in which the number of clusters is more distinct, whereas histograms are more efficient when dealing with larger, indexed colour spaces [25].

Owing to the clustering approach adopted by the POD system, GMM representation seemed better suited to representation and matching of object colour classes.

6.3.2 Expectation-Maximisation Training

Training of GMMs has been efficiently tackled by the Expectation-Maximisation method (EM) [29]. The input parameters to EM training consist of: a set of input data points $\mathbf{F}$; a set of initial Gaussian centres $\mathbf{C}_{1..m}$ and priors $\mathbf{P}_{1..m}$ (conventionally

set to be equal); and a log likelihood error threshold E_{thresh} which is used to terminate the training process. Training is divided into two steps: the E-step (Expectation, involving the evaluation of the posterior probabilities); and the M-step (Maximisation, where the centres are adjusted to the weighted means of the data). E- and M-steps are repeated until the log likelihood error E is below the threshold. For our purposes we demonstrate simple EM training for Gaussians with spherical covariance matrices.

The posterior $P(\mathbf{F}_n|\mathbf{C}_i)$ for each element of $\mathbf{F}$ calculated by the E-step is achieved in a similar manner to Equation 6.4, with the difference that the kernel activations are weighted by the priors (the tendency of each class to be favoured):

$$\mathbf{P} = [P_1 \dots P_m] \qquad (\text{where} \sum_{j=1}^{m} \mathbf{P}_j = 1) \tag{6.5}$$

$$P(\mathbf{F}_n|\mathbf{C}_i) = \frac{K_{\mathbf{F}_n\mathbf{C}_i}\mathbf{P}_i}{\sum_{j=1}^{m} K_{\mathbf{F}_n\mathbf{C}_j}}. \tag{6.6}$$

The subsequent M-step is thus completed by calculating the new priors $\mathbf{P}'$ and the means of the data points weighted by the posterior probabilities to produce a new estimate for the centres $\mathbf{C}'$. The updates for prior $\mathbf{P}_i$ and $\mathbf{C}_i$ are:

$$\mathbf{P}'_i = \frac{1}{N}\sum_{j=1}^{N} P(\mathbf{F}_j|\mathbf{C}_i) \tag{6.7}$$

$$\mathbf{C}'_i = \frac{P(\mathbf{F}|\mathbf{C}_i)\mathbf{F}}{\mathbf{P}'_i}, \tag{6.8}$$

where N is the number of feature points in $\mathbf{F}$. The error E is calculated as the negative log likelihood defined by:

$$E = -\sum_{j=1}^{N} \ln(P(\mathbf{F}_j|\mathbf{C})). \tag{6.9}$$

6.4 Extended Features

Although colour is the primary feature extracted from the pixel data, several region-based features are additionally measured for representing the spatial relations of the colour clusters. For region mask M bounded by box B, these are:

- Aspect ratio of bounding box: $\text{AR} = \frac{\text{Length}(B)}{\text{Width}(B)}$
- Rectangularity: $\text{RT} = \frac{\text{Area}(M)}{\text{Area}(B)}$.

In addition, the following sub-features are inferred from the set of observed colour features $\mathbf{F}$:

- Consistency: $\text{CT} = \frac{\text{Total matches}}{\text{Total observations}}$
- Proportional area: $\text{PA} = \frac{\text{Area}(\mathbf{F}_n)}{\text{Area}(M)}$.

These are then combined into an auxiliary feature vector set $\mathbf{F}_{aux}$ (Equation 6.10) and are used to aid matching:

$$\mathbf{F}_{aux} = [\text{AR, RT, CT, PA}]. \tag{6.10}$$

6.5 Network Synchronisation and SQL Databases

One of the aspects of the POD framework is the distributed processing model which can allow multiple processing nodes to share the object models. This implies that the representation must be both compact and easily synchronisable between processing nodes.

An extremely useful development in network information exchange has been the development of distributed relational databases. Data is stored in index tables with

each row in a table representing an entry which ties several columns of various information together. Additional tables can then link further information to specific rows in other tables simply by referencing its primary index. Such a relational representation is constructed by the DDL (Data Definition Language) and is referred to as a schema [37]. Information can then be selected and modified via a DML (Data Manipulation Language) script which targets any rows matching the script's criteria. Search queries are handled by a query language which in turn is closely related to the DML. The database is thus a storage block which provides data access by creating indexed trees, hash tables, and caches, thereby enabling the search queries to be more efficiently executed. Some primary advantages of database storage system over regular file systems include:

- Relational data abstraction
- Reduced data redundancy
- Data integration
- Network accessibility
- Concurrent-access handling
- Increased security.

One of the most predominant database scripting languages is SQL (Structured Query Language). The ANSI/ISO standardised version of the language, SQL-92, has evolved beyond its original creation by IBM in the early 1970's to a fully-fledged database management language encapsulating DDL, DML, as well as query functionality.

Generally, there are two classes of fields for storing information in a database. The first involves using the *blob* field which allows a block of binary data to be stored as is (eg. image data). The second option is to store the row as a vector array of various data columns (eg. integer, double, string). While storing data is equally easy

in both cases, blob fields are static, cannot be sub-searched, and are not as optimally retrievable by the query language.

Since the POD feature vectors intrinsically encapsulate the modelled data, synchronisation of models can be directly converted to a series of SQL row tuples. The main storage node depicted in Figure 3.3 can therefore be implemented by a standard SQL database. Processing nodes can then update local model repositories by simply querying the desired feature classes.

6.6 Implementation

The implementation of the POD training method deviates somewhat from the conventional EM method described previously. The main difference is the use of sequential rather than batch training. This was chosen so that intrinsic relationships of feature clusters could be analysed incrementally, allowing the number of training centres to be automatically estimated. A conventional approach to estimating the number of centres involves repeatedly running a fast clustering algorithm, like K-Means, using a different number of centres. The configuration which produces the least mean error is then refined using the EM process. In the case of the POD system, the number of centres can change as the number of observations increases, so a static parameter cannot be estimated in this way.

The POD procedure therefore begins by calculating the distances between the presented observation and the list of current centres (batch operation). Training then progresses by either assigning features to a matching cluster or initialising a new one. Figure shows 6.1 an overview of the training procedure.

If the current feature falls within k_{train} standard deviations of variance σ^2_{train} of its nearest centre, it is assigned to that cluster. The cluster's hit and consistency counter are updated and the centre is adaptively updated towards the new feature. The weighting α of the adaptation is determined by the ratio of the feature's area over

1. Calculate squared distance D^2 between observation features $O_{1..n}$ and training centres $C_{1..m}$.
2. For $i = 1$ to n

   if $\min(D^2(O_i, C_{1..m})) \leq (k_{train}\sigma_{train})^2$ (for C_j)

   Mark C_j as found.
   Increase C_j hit counter.
   Adapt C_j towards O_i proportional to ratio of their areas.
   Add area(O_i) to C_j.

   elseif $\min(D^2(O_i, C_{1..m})) > (nk_{train}\sigma_{train})^2$ AND area(O_i) $> a_{thresh}$

   Initialise new centre for O_i.
   Recalculate D^2.
3. Refine estimates with EM method.
4. Adapt aspect ratio.
5. Adapt proportional areas.
6. Drop centres whose proportional areas contribute to less than 1%.
7. Apply trained class to local repository.

Figure 6.1: *POD Training Procedure*

the area associated with the centre. Therefore instead of training the centres to the actual mean of the data, an importance ranking is established where larger areas are deemed more dominant. Finally, the cluster's area is updated by adding the newly matched feature's pixel area.

Should an input feature not match, but be more than two standard deviations from all current centres and meet a minimum area threshold, a new cluster is created. In this event, the distances between the input features and cluster centres must be recalculated.

After the model has been estimated, several iterations of EM can be used for refinement. During online model adaptation, the EM method can be used exclusively (skipping step 2) since the number of centres is unlikely to change significantly. The final phase of training is to adaptively update the auxiliary features, namely the bounding box aspect ratio and the area proportionality. Lastly, features which contribute less than 1% of the object's total area are discarded in order to reduce the system's sensitivity to noise. The resulting trained feature clusters are then stored in the local training repository.

6.7 Limitations

In order to ensure that CIELAB differences relate identically between clusters, a limitation must be imposed on the final class priors. For instance, having several different colour classes whose spheres of influence are different would result in the uniformity of the CIELAB space being compromised. Therefore, the POD system fixes the width of each cluster to the specified σ_{train}. While this encourages some overlapping of the cluster centres for small σ_{train}, this has little effect on the overall matching process.

Chapter 7

Matching and Classification

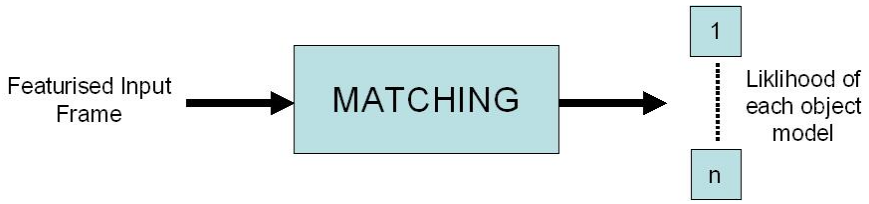

The central functional core of the POD system resides within the matching process. It is responsible for optimally extracting areas within an input image corresponding to each model in the repository. Since the entire system performance depends on its efficiency, the matching process cannot involve an exhaustive search of all models over all combinations throughout the entire image. Rather, relevant models need to be identified early and unrelated areas must be discarded as soon as possible. In this way, matching follows a process of elimination until a good comparison can be made.

In order to aid understanding, this chapter illustrates the matching process by means of a cartoon example. Cartoon characters, having well defined colour profiles, are relatively simple to match and allow for a more intuitive understanding of the overall process. The example comprises a single frame from a South Park[1] cartoon in which the character Cartman, shown in Figure 7.1, is matched.

Training a colour model for the character results in seven colour centres. A more

[1] All South Park material is copyright by Comedy Central.

Figure 7.1: *Matching target: Cartman character from South Park cartoon.*

detailed account of the training for this sequence is discussed later in Section 8.2, which deals with parameter tuning.

7.1 Overview

Matching is divided into several stages. Each stage targets a specific interpretation of the presented data which, when combined, produces a classification likelihood of an image region for a particular object model.

The process begins by performing colour matching on the set of input features $\mathbf{F}$ produced by pyramid segmentation. This basically assigns each feature to the nearest model centres[2] in the repository $\mathbf{C}$ (an $m \times 3$ matrix). For the cartoon example, there is only one target object, so $\mathbf{C}$ is a (7×3) matrix. The result is a list of active model centres $\mathbf{X}$ and their centroids in image co-ordinates. Since it is likely that certain colours will match a variety of different objects, an object model confidence is constructed based on:

- Quality of the colour match
- Variety of model features matched
- Spatial density and size of the features in image space

[2]This is a one-to-many relation since several object models might claim to match a single feature.

- Consistence of area proportionality.

Simply put, an object is likely to be found in a spatial cluster in which the colour match and the variety of centres is a maximum. Furthermore, the proportional areas of the features in the cluster must be comparable to the object model's ratios. If several of these measures agree, a peak in the likelihood will appear for a certain image region. If the overall confidence exceeds a lower threshold, the object is marked as found.

7.2 Colour Matching

As with the training procedure, colour matching is done using the CIELAB distances between the extracted features **F** and object model centres **C**. Equation 7.1 defines the Euclidean distance for two features (as in Equation 6.2). **X** is then defined as the matched subset of features, which are less than $k_{match}\sigma_{match}$ Euclidean units from any of the m model centres in **C**:

$$D^2(\mathbf{F1}, \mathbf{F2}) = (F1_{L*} - F2_{L*})^2 + (F1_{a*} - F2_{a*})^2 + (F1_{b*} - F2_{b*})^2 \quad (7.1)$$

$$\mathbf{X} = \{\mathbf{x} \in \mathbf{F} : D^2(\mathbf{x}, \mathbf{C}_i) \leq (k_{match}\sigma_{match})^2, \text{ for } 1 \leq i \leq m\}. \quad (7.2)$$

Colour matching is thus effectively a nearest neighbour classification.

7.3 Confidence Measurement

Estimation of the confidence measurements across a 2-D image plane requires evaluation of the contribution of each matched feature for each measurement of every object class. The fact that each object feature is only represented by a central pixel dictates that a sliding window operation is needed. Unfortunately this would result in an exceptionally high computational complexity since the convolution would need

to be repeated for each object class [39]. While this process can be improved using FFT fast convolution, the computational time is still proportional to the number of measurements and classes.

Therefore a less precise (yet efficient) idea is to perform measurement using a 1-D scanning algorithm which can be executed separately across the image's x and y directions. There is a possibility that a better approach might be to evaluate image quadrants [44] and use fast integral image convolution with boxlets [38]. However, separate class processing would still be required and so this alternative is left for future exploration.

Scanning proceeds by dividing the image into several evenly spaced, vertical and horizontal strips as shown in Figure 7.2(a). The matched features $\mathbf{X}'$ falling within a strip d_i then contribute to some property measurement $z(d_i)$ for each object model. When the measurements of all strips are concatenated, the results are two 1-dimensional likelihood signals $(\mathbf{z}_x, \mathbf{z}_y)$ spanning the width w_{im} and height h_{im} of the image respectively. Each signal is then filtered with a Gaussian kernel to smooth the disparity between the divisors (Parzen's method). Finally, the matrix multiplication of each object model's $\mathbf{z}_x$ and $\mathbf{z}_y$ vectors produces a 2-D likelihood map $\mathbf{L}_r$ for that object.

This method allows the confidence measurements to be tailored to specific areas for each image dimension. For instance, the proportionality measure holds little significance for person models in the horizontal direction since clothing divisions tend to appear vertical. As each measurement vector is one dimensional, multiple object models can be measured and stored in separate columns simultaneously. The result is an array of multi-model confidence measures created by a one-pass scan of the input image.

The following subsections describe each component measurement and show examples (Figure 7.4) calculated for the horizontal divisions of Figure 7.2(a). In order for the measurements to be combined equally, each measurement is configured to fit the range of $(0, 1)$ where 1 is the best match. The image in figure 7.2(a) is therefore used as a basis for the working example in the next several sections.

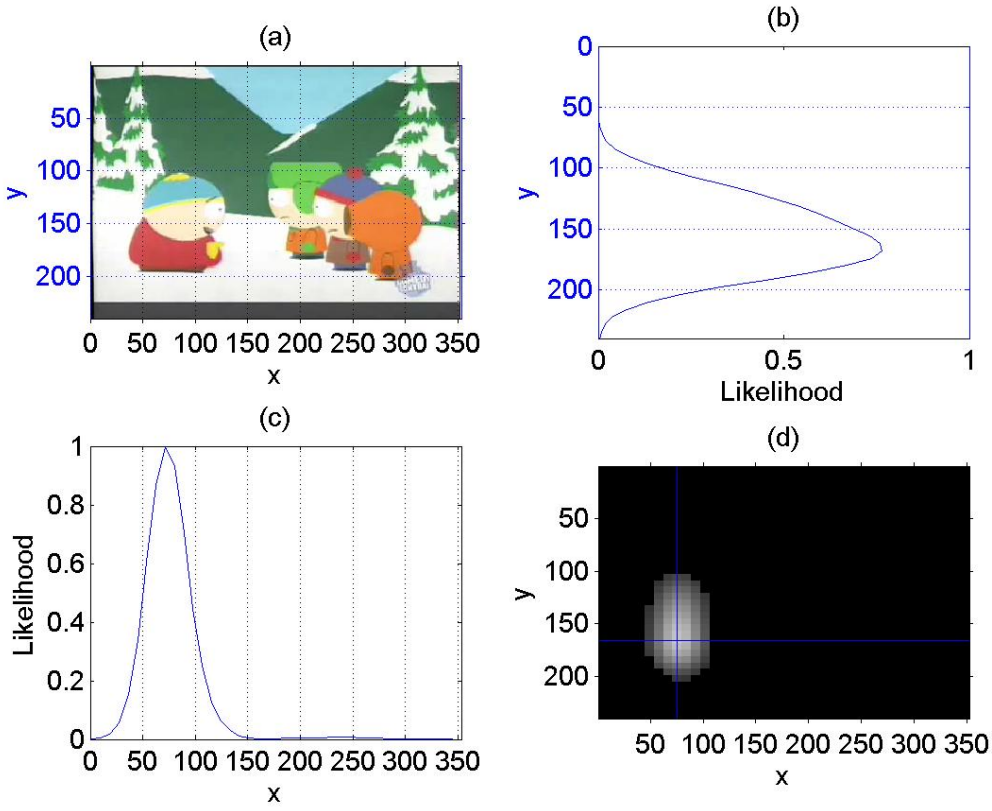

Figure 7.2: *Creation of the likelihood map. Image (a) shows the image divisions; Graphs (b) and (c) show the 1-D measurement signals in the y and x directions respectively; and image (d) shows the likelihood map for the trained character.*

7.3.1 Likelihood Map

The 2-D likelihood map $\mathbf{L}_r$ for each object r is generated by the matrix multiplication of the smoothed[3], overall confidence measurements $\mathbf{z}_x$ and $\mathbf{z}_y$ (Equation 7.5). These measurement vectors are constructed by the scalar multiplication of four measurement

[3]Smoothing is achieved using a Parzen window.

components:

$$\mathbf{z}_x = \mathbf{z}_{c_x}.\mathbf{z}_{v_x}.\mathbf{z}_{a_x}.\mathbf{z}_{p_x} \tag{7.3}$$

$$\mathbf{z}_y = \mathbf{z}_{c_y}.\mathbf{z}_{v_y}.\mathbf{z}_{a_y}.\mathbf{z}_{p_y} \tag{7.4}$$

$$\mathbf{L} = z_0(\mathbf{z}_x\mathbf{z}_y^{\mathrm{T}}), \tag{7.5}$$

where z_0 is a scaling factor and $\mathbf{z}_c, \mathbf{z}_v, \mathbf{z}_a, \mathbf{z}_p$ are the measurement components relating to quality, variety, area and proportionality respectively. In addition each component is the concatenated vector of the measurements for all divisions. For instance, if there are i divisions, $\mathbf{z}_{c_x}$ would consist of:

$$\mathbf{z}_{c_x} = [\mathbf{z}_{c_x}(d_1), \mathbf{z}_{c_x}(d_2), \ldots, \mathbf{z}_{c_x}(d_i)]. \tag{7.6}$$

Subsequently, $\mathbf{L}$ would then be an $(i \times i)$ map, similar to the example in Figure 7.2(d)[4]. Figure 7.4 shows the component measurements as well as the smoothed overall confidence $\mathbf{z}_x$ for the trained character.

Naturally, the number of divisions i does not have to be the same for each direction. In fact, for person tracking it can sometimes be better to allocate larger division spaces in the y direction since people are more rectangular. Note, however, that the actual division size in pixels is dependent on the size of the image dimension. Since most images are not square, this means that allocating the same number of divisions for each image dimension will not necessarily result in square likelihood regions. Generally, retaining the aspect ratio of the image is desirable, so using equal divisions for each dimension can be useful.

7.3.2 Quality of colour match

The first measurement component quantifies the quality of the average colour match $z_c(d_i)$ between $(n \times 3)$ feature subset $\mathbf{X}'$ (the matched features falling within d_i) and

[4]The likelihood map in the figure has been resized to be consistent with the image co-ordinates.

its corresponding matched object model centres $\mathbf{X'C}$ (i.e. $\mathbf{X'}$ and $\mathbf{X'C}$ are the same size):

$$z_c(d_i) = \frac{1}{n}\sum_{j=1}^{n} e^{\left(\frac{-D^2(\mathbf{X'}_j,\mathbf{X'C}_j)}{2\sigma^2_{match}}\right)}, \tag{7.7}$$

where D^2 is the Euclidean distance function defined in Equation 7.1.

Figure 7.4(a) shows the horizontal component of the quality measurement for the same image as shown in Figure 7.2(a). Although there is a slight peak on the left of the graph, the quality measure provides very little insight in this case. This is because we are processing an unsegmented image and the cartoon uses a small set of indexed colours which repeat throughout the scene.

7.3.3 Variety

If $\mathbf{X'}$ is the subset of matched features $\mathbf{X}$ falling within division d_i, then $\mathbf{h}_{d_i}(\mathbf{X'})$ is the histogram of feature areas for each object model centre in $(m \times 3)$ matrix $\mathbf{C}$ (within that division). The variety measure $z_v(d_i)$ is defined as:

$$\mathbf{v}_{d_i}(\mathbf{X'}) = \begin{cases} 1 & \text{for } \mathbf{h}_{d_i}(\mathbf{X'}) > h_{thresh} \\ 0 & \text{otherwise} \end{cases} \tag{7.8}$$

$$z_v(d_i) = \frac{1}{m}\sum_{j=1}^{m} \mathbf{v}_{d_i}(\mathbf{X'})_j. \tag{7.9}$$

The threshold h_{thresh} determines how many hits a bin requires before it qualifies for measurement (generally set to 1). Effectively the variety measure determines what fraction of the object model's centres is visible for each division. This relates to how much of a model is visible. Figure 7.3 shows the variety of each object centre across all horizontal divisions for the target object.

Each row represents one of the seven object model centres while the columns show the horizontal image co-ordinates (1 to 352 in this case). Coloured regions show the positive horizontal locations of each colour centre (colours match the actual object

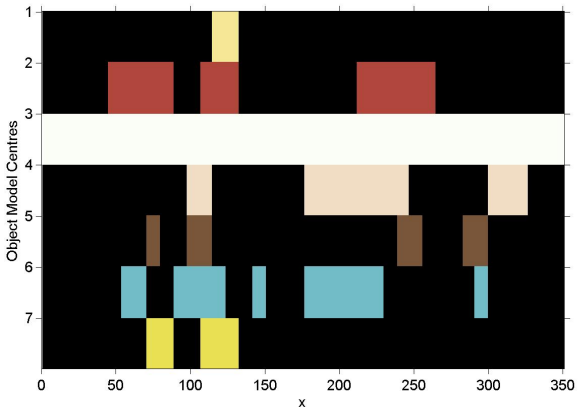

Figure 7.3: *Variety of object centres across the horizontal image dimension. Object model colours are shown for positive matches of each centre.*

model centres). A high variety will be detected where most of the object centres overlap for a particular x value. Clearly, the white class is not a good descriptor in this case since it is detected throughout the image. Figure 7.4(b) shows the full summed horizontal variety measure $\mathbf{z}_{v_x}$. In the example, the maximum variety occurs approximately $x = 100$ which is seen in Figure 7.3 where the most centres have been matched.

7.3.4 Area Distribution

The distribution of feature areas can also hold vital information about the whereabouts of an object. Once again, $\mathbf{X}'$ is the n feature subset of $\mathbf{X}$ falling within d_i, and the area distribution $z_a(d_i)$ is:

$$z_a(d_i) = \frac{1}{A_{max}} \sum_{j=1}^{n} \text{area}(\mathbf{X}'_j), \tag{7.10}$$

where A_{max} is the maximum feature area throughout the image. This measurement serves to identify the division that holds the greatest area of matched pixels. The example plot in Figure 7.4(c) shows that the area distribution measure performs poorly as a descriptor for the object model. This is due to the vast repetition of

colour throughout the unsegmented image, causing noise in the measure.

7.3.5 Proportionality

Proportionality refers to the ratio of the mixture of colour features for a particular object model. Often, several background regions can match a particular object's colours (seen in previous measurements), however the true object can be isolated by analysis of the proportions of these colours. The proportionality measurement is defined by the Chi-Square distance (Equation 7.13) between the area histograms $\mathbf{h}_{d_i}(\mathbf{X}')$ (from Equation 7.8) and $\mathbf{h}_{d_i}(\mathbf{C})$ (areas of object model centres) within division d_i. The histograms each have m bins which relates to the number of model centres for the specific object and are each normalised by their total sum. The Chi-Square distance provides a comparative metric between distributions and maps the interval $(-\infty, \infty)$ to $(0, 1)$ (where 0 is a close match). To make the values consistent with the other measurements (0 — no match, 1 — best match), the Chi-Square distance is subtracted from 1. Proportionality measurements $z_p(d_i)$ therefore fall within the $(0, 1)$ range where 1 is the closest possible match (Equation 7.14).

$$\mathbf{h}'_{d_i}(\mathbf{X}') = \frac{\mathbf{h}_{d_i}(\mathbf{X}')}{\sum_{j=1}^{m} \mathbf{h}_{d_i}(\mathbf{X}')_j} \tag{7.11}$$

$$\mathbf{h}'_{d_i}(\mathbf{C}) = \frac{\mathbf{h}_{d_i}(\mathbf{C})}{\sum_{j=1}^{m} \mathbf{h}_{d_i}(\mathbf{C})_j} \tag{7.12}$$

$$d^2_{Chi-Square} = \sum_{j=1}^{m} \frac{(\mathbf{h}'_{d_i}(\mathbf{X}')_j - \mathbf{h}'_{d_i}(\mathbf{C})_j)^2}{\mathbf{h}'_{d_i}(\mathbf{X}')_j + \mathbf{h}'_{d_i}(\mathbf{C})_j} \tag{7.13}$$

$$z_p(d_i) = (1 - d^2_{Chi-Square}) \tag{7.14}$$

The proportionality plot shown in Figure 7.4(d) for the running example shows a peak in the area of the target object (approximately $x = 100$). This demonstrates how proportionality tends towards a maximum when the matched colour features occur with the correct proportions.

7.4 Importance Weighting

As seen by the resulting example measurement plots in Figure 7.4, it is highly likely that multiple objects will share common colours leading to uninformative measurements. In the example, the background scene contributes a fair amount of clutter which causes some of the measurements to lose validity. Therefore in order to ensure that the overall confidence measurement is not compromised, each feature must be weighted by its importance.

Importance is determined based on how common a feature is found to be spatially. For instance, the object centre variety plot in Figure 7.3 showed that the white class was common to the whole image, while the yellow features clustered in the vicinity of the target object. Therefore, the sensible approach would be to consider the yellow features more important than the others when constructing each measurement.

Calculation of the importance weightings $\mathbf{I}$ involves the estimation of the spatial variance of each model centre in $\mathbf{C}$ for the entire image. This is accomplished by calculating the proportional spatial range of each feature out of the whole image. The importance weighting I_a for an arbitrary object centre $\mathbf{C}_a$ is the sum of the number of occurrences h_{sum} of $\mathbf{C}_a$ across all divisions, divided by the total number of divisions i. This is calculated for each image dimension, averaged and then squared to produce an importance value in the range $(0, 1)$[5]:

$$I_{a_x} = \frac{h_{sum_x}}{i} \tag{7.15}$$

$$I_{a_y} = \frac{h_{sum_y}}{i} \tag{7.16}$$

$$I_a = \left(\frac{I_{a_x} + I_{a_y}}{2}\right)^2 \tag{7.17}$$

$$\mathbf{I} = (I_1, I_2, ..., I_m), \tag{7.18}$$

[5]A low importance corresponds to a low contribution of that object centre to the likelihood and visa versa.

where $\mathbf{I}$ is the vector of importance values $(I_1..I_m)$ for all object centres.

Importance weights are applied by multiplying each object centre in each measurement by its corresponding weighting. This also requires that the measurements are subsequently normalised by the sum of the object model's importance weightings in order to maintain the $(0, 1)$ measurement range.

Figure 7.5 shows the new measurements for the example after the importance weights have been applied. Importance weights are not applied to the proportionality measurement since it would create a meaningless result. The most noticeable improvements are in the quality and area distribution measures shown in Figures 7.5(a) and 7.5(c) respectively. Additionally, it is evident from the overall confidence $\mathbf{z}_x$ in Figure 7.5(e) that the importance weightings provide better discrimination in the presence of clutter (i.e. the second mode is completely removed).

7.5 Pan Tilt Zoom Extension

In the surveillance world, Pan Tilt Zoom (PTZ) refers to cameras which have a mobile axis and whose view can be controlled by rotating, tilting or zooming in order to monitor a scene. Owing to the fact that the POD matching method is not fully dependent on the static background segmentation, certain objects can be automatically tracked if their likelihood map is stable enough over a period of time.

A naive PTZ tracking algorithm has been added to the POD's functionality. Generally, PTZ tracking involves keeping the target object centred and well scaled within the image frame. Given a modelled object's best match from the likelihood map, the algorithm simply measures the x and y differences between the centres of the match and image frame. If the difference vector is outside a defined hysteresis window, an appropriate counter movement is generated. The PTZ then iterates one step in the corrected direction and the next match is calculated. This method allows the actual PTZ parameters to be ignored and simply moves the camera in the direction that

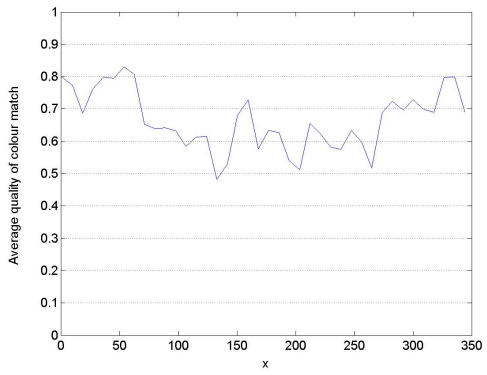

(a) Quality of colour match

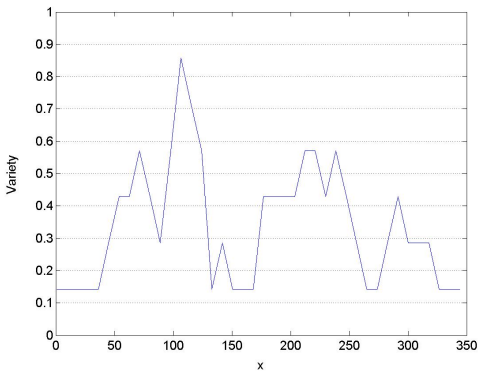

(b) Variety

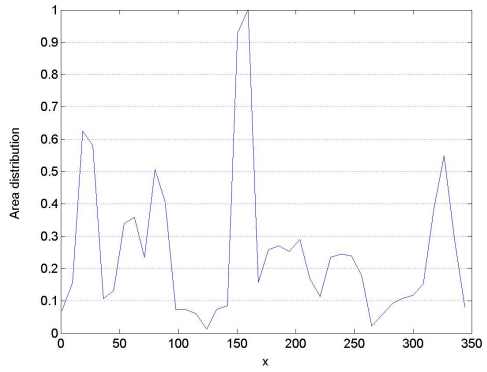

(c) Area distribution

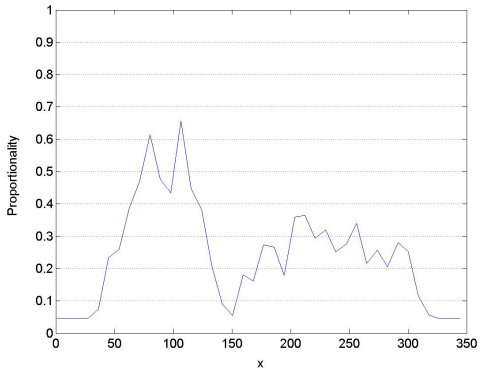

(d) Proportionality

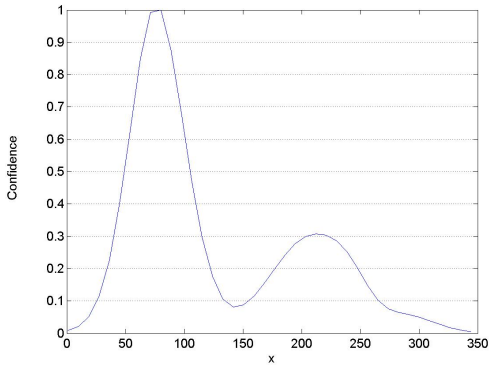

(e) Scaled overall confidence with smoothing

Figure 7.4: *Measurement components calculated for Figure 7.2* ***without*** *importance weighting.*

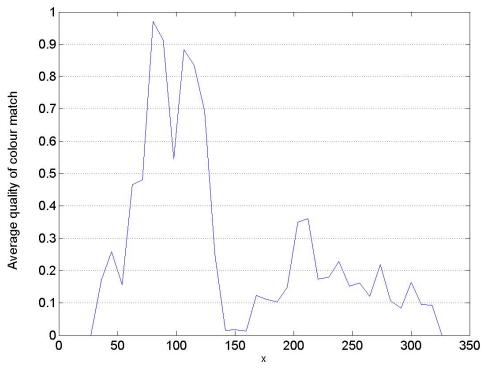

(a) Quality of colour match

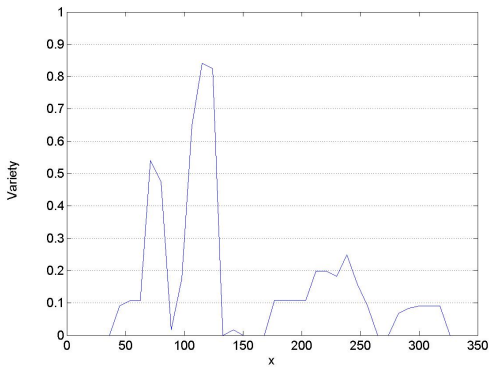

(b) Variety

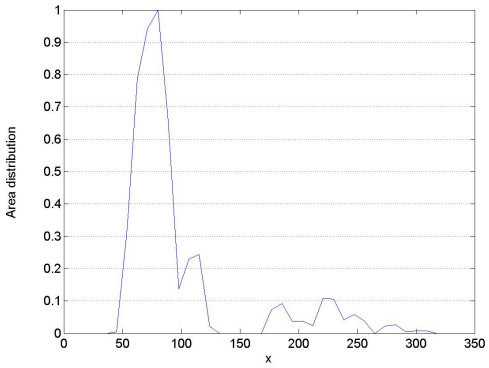

(c) Area distribution

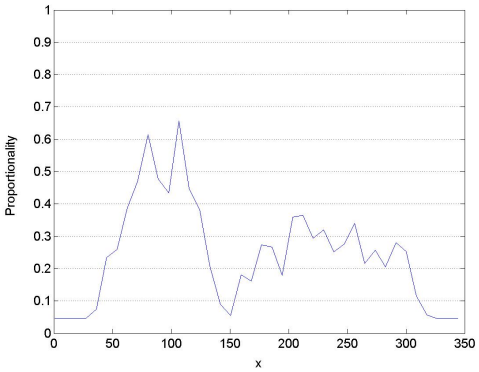

(d) Proportionality

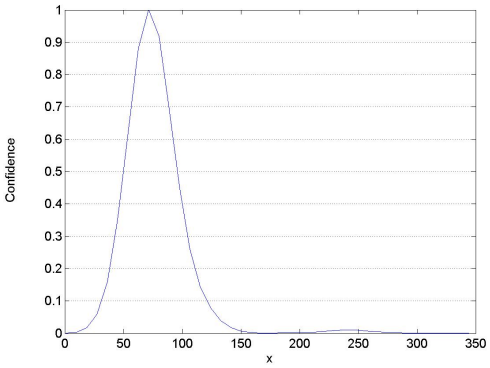

(e) Scaled overall confidence with smoothing

Figure 7.5: *Measurement components calculated for Figure 7.2* ***with*** *importance weighting*

will centre the likelihood map.

Figure 7.6 shows some frames from a live PTZ tracking sequence (the full sequence can be seen in Appendix C). The red ellipse identifies the matched image region while the green square represents the centred hysteresis window. In this case, the network latency and slow camera motors cause tracking to be too slow for regular human movement. However, this does not detract from the POD system's innate ability to compensate for lag.

Figure 7.6: *Example frames from a live PTZ tracking sequence.*

7.6 Implementation

Normally, the likelihoods for multiple object models would have to be generated separately so that separability remains intact. However, because of the nature of the measurement system, multiple object classes can be calculated simultaneously and

concatenated as rows. The only iterative process is the final multiplication of x and y measurement vectors that must be calculated for each object.

The actual implementation of the matching method previously described is straightforward and closely follows the previous sections. Once measurements have been constructed, a set of user parameters (fully described later in Section 8.3) determines which likelihood regions are extracted for the final output.

7.6.1 Interference filtering

Generally, it is likely that there will be a fair amount of measurement interference between similarly coloured object models. When dealing with a perspective camera view, this interference can cause the system to mistakenly detect several objects in the same location due to the possibility that they may be occluding one another.

In order to address this, a simple interference filtering scheme is implemented which ensures that only one object can occupy an image portion. Filtering proceeds by processing each detected object in descending order of likelihood. Each object likelihood is multiplied by a spread function which enforces its authority across the detected area while reducing the likelihoods of all interfering models. In simplistic terms, a notch filter is applied to each model. The width of each notch filter is automatically determined by the width of the detected likelihood.

As an example, consider Figure 7.7 which shows the x direction likelihood of several object models in a scene. Note the overall inter-class interference before and after filtering.

7.7 Limitations

One issue with the matching process relates to its 1-D formation of measurements. Occasionally, the separation of x and y information can cause a mismatch. When an

object is matched correctly in one dimension and incorrectly in the other, a phantom likelihood is created in an incorrect image area. Fortunately, this is fairly rare and only occurs when two objects are extremely similar. Future implementations should try to link the matching information between image dimensions, thus allowing better correlation of measurements.

A final limitation involves the use of interference filtering. Specifically, the method can only be applied when objects occlude each other in a perspective view. This is due to it depending on the nature of occlusions in the scene. For instance, were the technique used in a ceiling camera system, objects occupying the same orthographic spaces would cancel out, resulting in increased false negative matches.

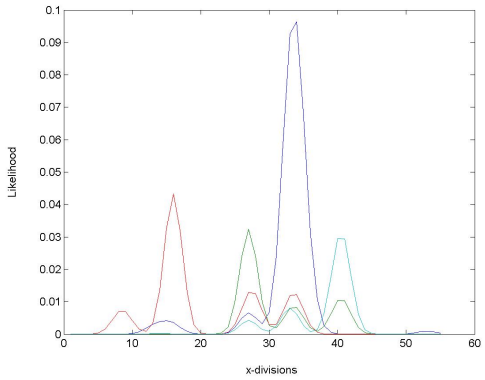

(a) Horizontal likelihood for 4 objects.

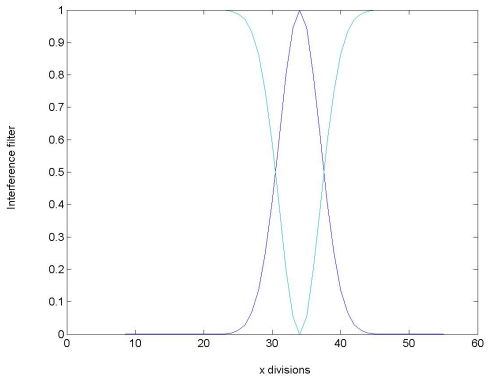

(b) Interference filter for best matched object.

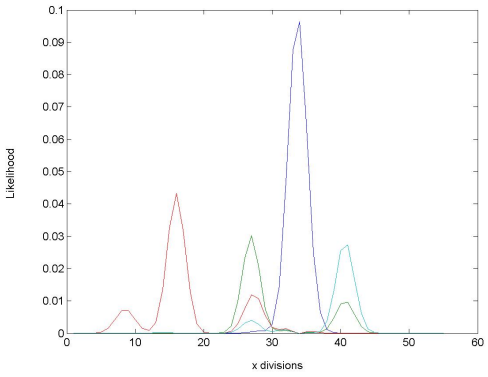

(c) Filtered likelihood for best matched object.

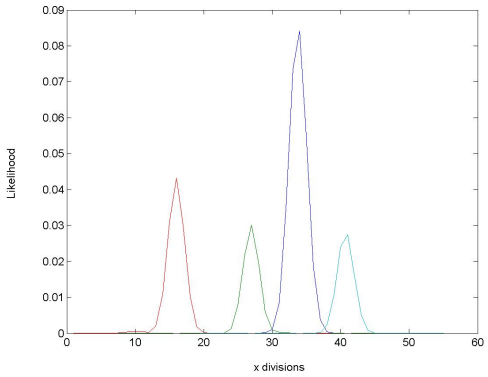

(d) Final likelihoods after all objects have been filtered.

Figure 7.7: *Interference filtering example.*

Chapter 8

Results

Acquiring meaningful results for a computer vision system is a difficult process. This arises from the fact that the exact definition of good performance varies between different types (and goals) of systems. Standard benchmarks are therefore extremely hard to come by and are generally only comparable when systems use similar test sequences.

In order to determine the overall performance and versatility of the POD system, several test sequences from different environments have been selected. Sections 8.4, 8.5 and 8.6 summarise the results of the system for each test case. It is rather difficult to grasp the extent of a vision system's performance without actually seeing it operate. For this reason the video results for each test sequence have been provided on the included CDROM (see Appendix C).

This chapter proceeds by first defining the performance metrics used for system evaluation. This is followed by a detailed walk-through of the parameter selection methods for both training and matching subsystems. The final section (after the test case results) consists of a discussion concerning the overall performance and limitations of the system.

Since the POD system combines both tracking and classification approaches, a variety of comparative methods are used to evaluate performance.

8.1 Performance Evaluation

A number of methods exist for evaluating the performance of vision systems. Even though the POD system is not entirely a stand-alone surveillance platform, it does exhibit certain similarities which warrant the use of some surveillance metrics.

8.1.1 Surveillance Metrics

The following basic metrics (taken from [4]) have been used to gauge overall system performance:

Tracker Detection Rate (8.1)

$$\text{TRDR} = \frac{\text{Total True Positives}}{\text{Total Number of Ground Truth Points}}$$

False Alarm Rate (8.2)

$$\text{FAR} = \frac{\text{Total False Positives}}{\text{Total True Positives} + \text{Total False Positives}}$$

Track Detection Rate (8.3)

$$\text{TDR} = \frac{\text{Number of true positives for tracked object}}{\text{Total number of ground truth points for object}}$$

Object Tracking Error (8.4)

$$\text{OTE} = \frac{1}{N_{rg}} \sum_{i=1}^{N_{rg}} \sqrt{\frac{(xg_i - xr_i)^2 + (yg_i - yr_i)^2}{w_{im}^2 + h_{im}^2}}.$$

The TRDR provides a general measure of the system's accuracy by describing the proportion of correct classifications for all frames in which ground truth is available. Similarly, the FAR determines how often the system claims an object is present when it is not. Since the system may generally perform better on some objects than others, it is useful to know the specific TRDR for each object. This is encapsulated by the TDR.

Finally, the OTE quantifies the overall system error by measuring the average error of the tracked path with respect to ground truth for each object model. The equation has been modified from its original form by adding the $w_{im}^2 + h_{im}^2$ denominator. This normalises the pixel error (numerator) to the length of the image diagonal which represents the largest possible error. N_{rg} is the total number of ground truth points, (xg_i, yg_i) are the object's ground truth co-ordinates at frame i, and (xr_i, yr_i) is the object's classified position point. It should be noted that because the POD system does not take into account the 3-D pose information of the camera and scene, all co-ordinate measurements are in image space, i.e. x and y represent columns and rows in the image matrix.

An additional measurement which has been defined, owing to the 2-D nature of the system, is the Object Area Error (OAE). This is effectively the the average area difference between the bounding boxes of classified objects and their corresponding ground truth areas:

$$\text{Object Area Error} \tag{8.5}$$

$$\text{OAE} = \frac{1}{N_{rg}} \sum_{i=1}^{N_{rg}} \frac{\text{area}(bbox_{g_i}) - \text{area}(bbox_{r_i})}{\text{area}(bbox_{g_i}) + \text{area}(bbox_{r_i})},$$

where N_{rg} is again the total number of ground truth points, and $bbox_{g_i}$ and $bbox_{r_i}$ are the bounding boxes for the ground truth areas and classified objects respectively. Defining the area comparison in this way produces a measure in the range $(-1, 1)$ where a negative value indicates that the classified bounding boxes tend to be smaller than the ground truth and a positive value, the opposite.

8.1.2 Perceptual Complexity

In order to compare surveillance metrics between different types of video sequences a quantitative measurement is needed to relate the intrinsic differences between each sequence. A reasonable approach is to define the Perceptual Complexity (PC) for a sequence (suggested by [4]). The PC describes how 'difficult' a sequence is in the

visual tracking sense. Generally, this is related to factors such as the number of objects to be tracked, the extent of occlusions, and image quality. For our purposes we define the perceptual complexity by:

Perceptual Complexity (8.6)

$$\text{PC} = w_1\text{OC} + w_2\text{CS} + w_3\text{QI} + w_4\text{NE}$$

Occlusion Complexity (8.7)

$$\text{OC} = \frac{1}{N}\sum_{i=1}^{\text{NO}} \text{OE}_i.\text{OD}_i$$

Colour Similarity (8.8)

$$\text{CS} = 1 - \frac{1}{100N}\sum_{i=1}^{N} \min(\sqrt{D^2(C1, C2)}), \quad (8.9)$$

where OC, CS, QI and NE describe the Occlusion Complexity, Colour Similarity, Quality of Image and Number of Exits respectively. Each term is within the range $(0, 1)$ and is weighted by an importance value $w_1...w_4$ (summing to 1) which determines how much each quantity contributes to the PC rating.

Occlusion Complexity (OC) is calculated by summing the mean Occlusion Extents multiplied by the Occlusion Durations (OD) in frames for the Number of Occlusions (NO). This value is then normalised by the total number of frames N.

The Colour Similarity (CS) term is estimated by averaging the minimum CIELAB distances between each combination of object model pairs, over the total number of models. Therefore, a set of objects whose colour profiles are very different will correspond to a large perceptual colour difference, while the average distance between similar objects will be small. The value is further normalised by the radius of the CIELAB sphere.

Quality of Image (QI) and Number of Exits (NE) account for average image variance, visibility and how enclosed the tracked area is. Although the NE factor is not relevant to the POD system, it has been retained in order to provide consistency with the

results of 3-D tracking methods. The weightings (w_1, w_2, w_3, w_4) assigned for the PC ratings in the results are [0.3, 0.3, 0.3, 0.1].

8.1.3 Ground truth

Performance evaluation of vision system is largely dependent on the availability of ground truth data. Naturally, since real-time video has a data rate of between 25 and 30 frames per second, creating ground truth is exceedingly time consuming. Methods for obtaining ground truth range from using semi-automated tools [9] to estimation (eg. silhouette fitting [36]) and use of consistency measurements [11].

Fortunately, since the sequences used for evaluation are not excessively long, manual ground truth[1] could be generated for each frame. Figure 8.1 shows a few example frames where each person's ground truth has been marked. The accuracy of the ground truth is not critical since the performance measurements only compare the bounding boxes.

Figure 8.1: *Examples of manually generated ground truth.*

[1]Courtesy of Markus Louw.

8.2 Training Parameters

Before we can ascertain the performance of the matching process, it is imperative that the consistency of the trained object models be verified. This is a difficult task since the results of the modelling procedure are only fully evident after matching is performed. In terms of the selection of colour groupings for an object, training progresses in an unsupervised manner. Therefore in order to quantify the consistency between a trained model and its actual object, test objects exhibiting low pixel variance with a finite number of colour classes were needed. This lead to the idea of using cartoon characters whose visual profiles remain nearly constant and allow a human user to more accurately estimate the optimum number of colour classes.

Figure 8.2 shows the images of four characters from the South Park[2] cartoon. The parameters which control the training are:

σ_{train}**:** The radius of influence for a particular colour class.

k_{train}**:** The number of standard deviations within which a colour must fall to be considered part of that class.

nk_{train}**:** The minimum distance required between a prospective class and the current set of class centres.

a_{thresh}**:** The minimum proportional area a prospective class must have before it is accepted.

From the images, the number of ideal colour classes can be estimated as being: 5; 5; 6; and 4, for each character from left to right and ignoring very small regions. The value of nk_{train} simply specifies how distinct each colour class will be. Generally marginal overlapping is desired so that no areas are unintentionally excluded. Therefore nk_{train} is set to be $2k_{train}$, which is the closest distance two centres can be without excess interference.

[2]All South Park material is copyright by Comedy Central.

Figure 8.2: *Test characters for training: Stan, Kyle, Cartman, and Kenny (from left to right).*

8.2.1 Rough Tuning

The first step is to analyse the result of changing σ_{train} and k_{train}. Figure 8.3 shows four graphs of varying sigma, for each value of k_{train} from 1 to 4.

Since a Gaussian curve is practically zero after $\sigma_{train} = 4$, there is little to be gained from exploring higher values of k_{train}. Each graph shows the number of detected colour classes for each character (left to right order) for σ_{train} from 1 to 15.

From the figure it is seen that the number of classes converges to the ideal range (between 4 and 6) as σ_{train} increases. Furthermore, k_{train} affects the rate of convergence for the range of sigma presented. Convergence is guaranteed due to the distance threshold nk_{train} which ensures that classes cannot split into small fragments.

8.2.2 Fine Tuning

The next step is to fine tune the parameters by monitoring the quantisation error of the trained colour classes to actual image pixels over the converged range. This will ensure that the number of colour classes corresponds to reasonable representations of the image data. The quantisation error is calculated by the mean CIELAB difference between the input image and the image where each pixel has been assigned its trained colour class. Figure 8.4 shows the quantisation error surface generated

The general trend is that σ_{train} and k_{train} are directly proportional to the quantisation

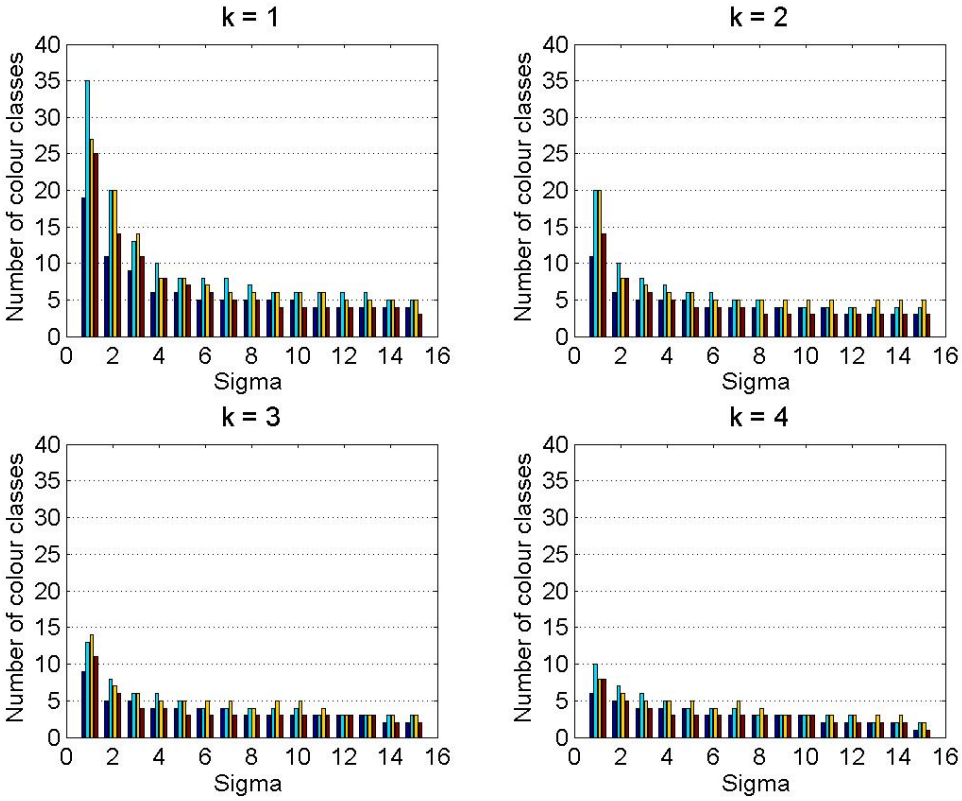

Figure 8.3: *Tuning training parameters. Each graph shows the results for* $k_{train} = 1$ *to* 4*. The number of trained colour classes per character is shown by the vertical bars and is evaluated for* σ_{train} *from 1 to 15.*

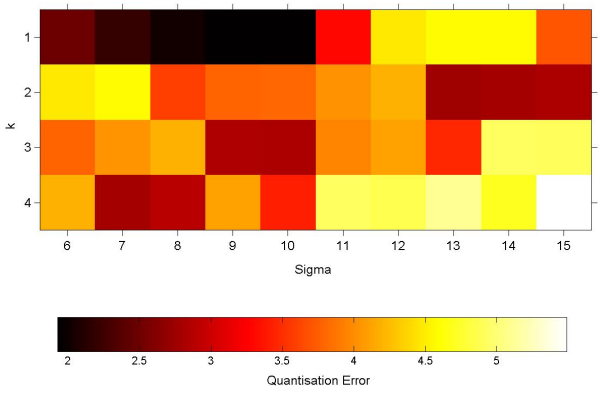

Figure 8.4: *Quantisation error between trained classes and actual pixel data versus the* σ_{train} *and* k_{train} *parameters.*

error. Minimisation of the quantisation error ensures the best object model approximation. This occurs at $\sigma_{train} = 9$ and $k = 1$. The surface also shows some anomalies where the quantisation seems low for high values of σ_{train} and k_{train}. These artifacts are created because the quantisation is an average over the four trained object models. Some of the characters are dominated by a single colour and since the training procedure processes regions in order of area (largest to smallest), the trained model captures the majority of the object with just one colour class. This results in a lower quantisation error, thereby affecting the mean value.

8.2.3 Detail sensitivity

The final tuning step is to set the area threshold a_{thresh}. This is specified as a factor of the mean region area. For instance, a value of $a_{thresh} = 1$ means that a new class is only added if it is bigger or equal to the average region area in the object. A small value for a_{thresh} will spawn an increase in the number of colour classes since smaller, insignificant regions will be included. Conversely, a_{thresh} values greater than one will reduce the number of colour classes. This parameter therefore tunes the sensitivity of the training process to regional pixel noise. Effectively this means that the parameter must be tuned to the type of video data being used, since pixel variance will vary depending on the camera hardware, lighting conditions, and average object size.

Figure 8.5 shows a plot of a_{thresh} versus the average number of colour classes detected. Care must be taken when selecting a_{thresh} in order to ensure that the number of classes is realistic. In general $a_{thresh} = 1.5$ provides a safe estimate. However, for the cartoon characters $a_{thresh} = 2.5$ results in the average number of classes matching the ideal case, and in fact each object is divided perfectly resulting in 5, 5, 6 and 4 colour classes for each character respectively.

The resulting trained colour classes for each character are shown in Figure 8.6. Perceptually, the colour groupings make sense compared with the example images shown in Figure 8.2.

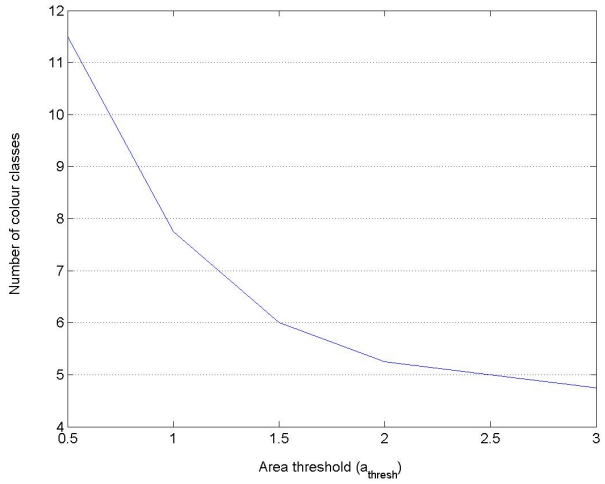

Figure 8.5: *Tuning of area threshold. A value of* $a_{thresh} = 2.5$ *provides a reasonable estimate to the ideal value for the cartoon characters.*

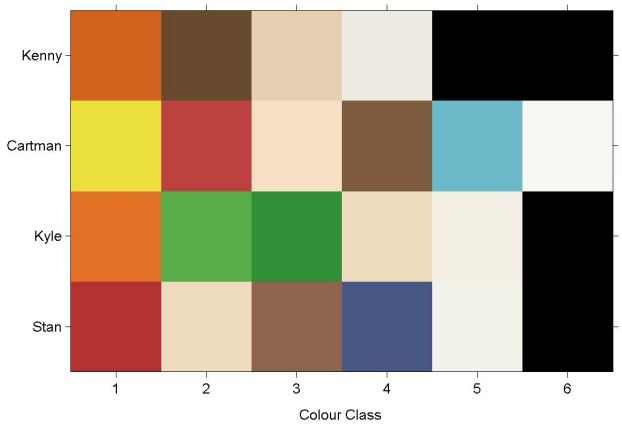

Figure 8.6: *Resulting trained colour classes for each character.*

8.3 Matching Parameters

In contrast to the training step, the matching parameters are far more sensitive to the type of video environment. This stems from the differences in image quality between various camera/capture hardware as well as the camera pose and lighting settings. The matching controls have been divided into three groups:

- Colour matching parameters
- Object matching parameters
- Switches.

Although the exact parameter selection does vary slightly for different scenarios, the selection method is very basic. Therefore in order facilitate explanation, the familiar cartoon example has been extended to illustrate the matching process. Owing to the nature of the animation (camera is unconstrained and changes pose), motion segmentation is not achievable and has been omitted thus raising the difficulty of matching.

8.3.1 Colour matching parameters

The colour matching parameters stipulate the thresholds for matching a colour feature to an object model centre. As with training this is specified by:

σ_{match}**:** The radius of acceptance for a particular colour class.

k_{match}**:** The number of standard deviations within which a colour must fall to be considered part of that class.

Since the colour matching process is identical in both the training and matching subsystems, it is logical to assume that using the same parameters should be acceptable. One consideration is the subject of image variance. Generally, a person will

change appearance slightly (and sometimes greatly) depending on his position and the lighting changes in an environment. Even though the trained object models can be adapted at each stage, it was found that a better (and more efficient) approach is to only adapt the model occasionally and to compensate variance by extending the width of matching with respect to training. Therefore σ_{match} remains the same between training and matching, while $k_{match} = 3$ is used in matching. Since the quality measurement incorporates this distance between colours, a balanced result is obtained because colours with higher variance are matched, but their likelihood contribution is lower.

Figure 8.7 shows an example of matching an unsegmented frame to the four character models trained in the previous section. Note the background clutter created by using an unsegmented input.

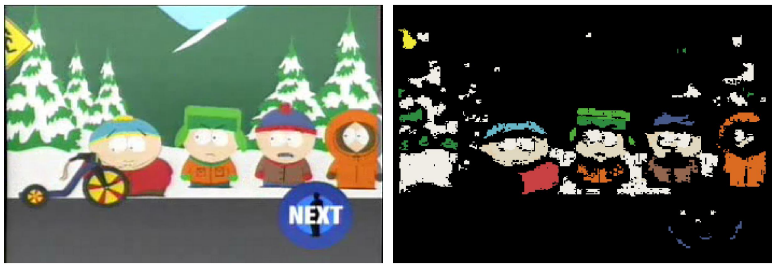

Figure 8.7: *Example output of colour matching process. The left hand image shows the original input, while the right hand image shows which colours have been matched to character models.*

8.3.2 Object matching parameters

Object matching parameters control the threshold levels of detection as well as the division and smoothing settings. These are:

(dx, dy)**:** The number of dividing strips over which the confidence measurements are calculated in the horizontal and vertical image directions respectively.

$(\sigma_{dx}, \sigma_{dy})$**:** The width of each smoothing Gaussian that is applied over the horizontal and vertical measurement vectors.

$m1_{thresh}$**:** The minimum probability that is required for a likelihood area to be considered a match.

$m2_{thresh}$**:** The minimum area of a likelihood area required for a match.

Selecting the number of divisions

The values of dx and dy specify the number of divisions, therefore each division is $\frac{im_w}{dx}$[3] (for the horizontal direction) and $\frac{im_h}{dy}$ (for the vertical direction) in pixels respectively. The effect of adjusting the number of divisions relates proportionally to the output resolution of the likelihood map. Basically, it defines the minimum detectable object size. A small value will tend to expect large objects and cause merging between object classes within close proximity. Conversely, a large division number will give a high-definition likelihood, but can cause object fragmentation.

In Chapter 7 it was shown that the measurements are calculated for each discrete division bin. In order to produce a smooth, unbiased response, the horizontal and vertical measurement vectors are thus smoothed with a Parzen window. The values σ_{dx} and σ_{dy} specify the width of the Gaussian used for this smoothing operation and are specified as a per unit fraction of the length of the respective image dimension. These parameters are fixed to a minimum width which will provide smoothing without deteriorating the measurement vector's distribution. Values of $\sigma_{dx} = \sigma_{dy} = 0.2$ have been found to provide effective smoothing for all test cases.

Figure 8.8 shows the detected object areas for the four example characters for $dx = dy$ taking on values 10, 50, 100 and 200 divisions respectively. As predicted, $dx = 10$ provides a very wide, general object detection area which overlaps with nearby classes. On the other hand, $dx = 200$ produces a very fine search window, which in this case causes target loss since the object features are spread too thinly. Plotting the area

[3]Values im_w and im_h correspond to the image width and height respectively.

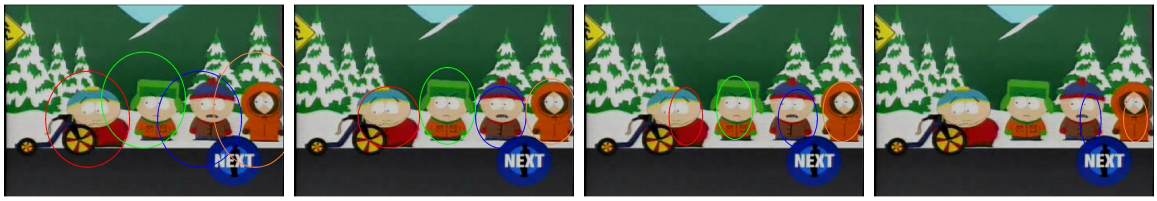

Figure 8.8: *Detected object areas for dx = dy taking on values 10, 50, 100 and 200 (divisions from left to right).*

error between the ground truth and the detected targets (OAE) versus the divisions parameter results in the curve shown in Figure 8.9.

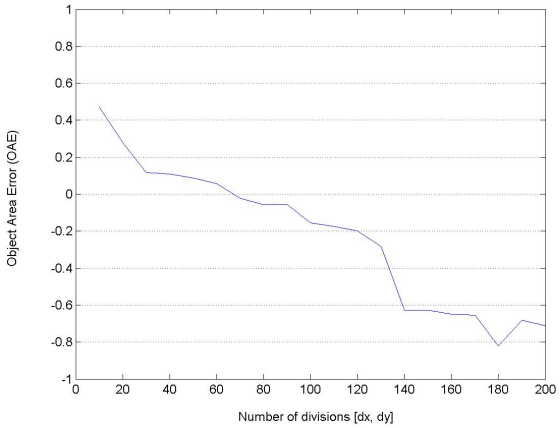

Figure 8.9: *Object Area Error (OAE) plotted against varying number of divisions.*

A positive OAE value shows that the detected area is larger than the ground truth while a negative value indicates the reverse case. As seen, the minimum error is obtained at approximately $dx = dy = 70$. While this parameter should be tuned to the type of video scene, generally $dx = dy = \frac{im_w}{4}$ is a reasonable starting point.

If dx is not equal to dy, the result is that one image dimension produces a wider response. This can be useful if there are constraints on the type of objects being matched (eg. standing people are longer vertically). In general, it is best to keep $dx = dy$ so that no assumptions are made about object pose and the image aspect ratio is maintained.

Detection thresholds

The final set of matching parameters consists of the likelihood level detection thresholds. These are applied to the combined likelihood map of for all object classes.

The area threshold $m2_{thresh}$ specifies the minimum area required for a likelihood region to be matched. This is simply set to the smallest possible object pixel area and serves to filter out detection of spurious regions. Values of $10 \leq m2_{thresh} \leq 50$ encompass the general range used in the test cases.

The most relevant parameter in matching is the likelihood threshold $m1_{thresh}$. This determines the lowest maximum match likelihood value necessary for a positive match. A number of external factors affect selection of this parameter. The most relevant factor is the average quality of colour matches in the scene, which relates directly to camera iris and gain controls on top of scene lighting conditions. The worse the 'visibility' of the scene, the lower the average match likelihood. Tuning of the likelihood threshold determines the exact matching performance of the system. The best performance (highest TRDR) will occur when the lowest ratio of false positives to false negatives is reached. This is illustrated by means of an ROC curve. Figure 8.10 shows a generated ROC curve obtained for 50 frames of the cartoon example where $m1_{thresh}$ has been varied between 0 and 1.

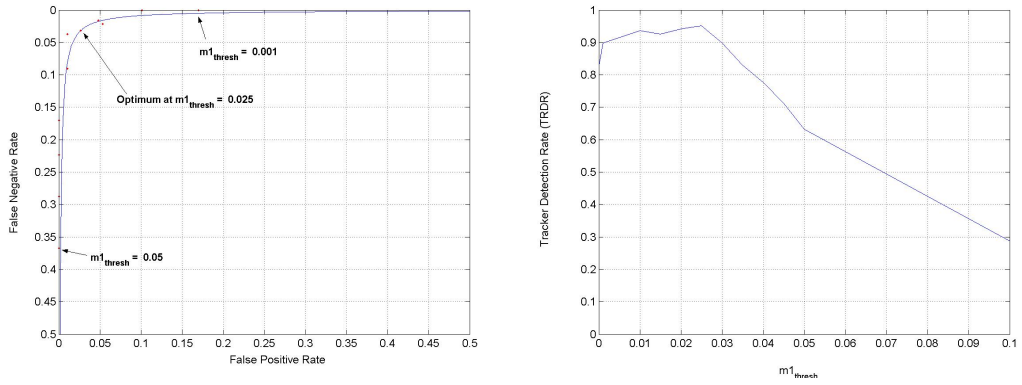

Figure 8.10: *Left: ROC curve for 50 frames of cartoon sequence for* $0 \leq m1_{thresh} \leq 1$*; Right: Tracker Detection Rate (TRDR) for the same range of* $m1_{thresh}$.

The second graph in Figure 8.10 shows the corresponding Tracker Detection Rate (TRDR) for the same sequence. The reason for the high performance value is related to the low lighting and colour variance inherent in cartoon sequences (which is why it was used as a first trial). Owing to the multiplicative creation of the likelihood map ($\mathbf{z}_x\mathbf{z}_y^T$ from Equation 7.5), the likelihood has a steep falloff thereby producing a very low dynamic range for threshold tuning. Selection of $m1_{thresh}$ therefore requires manual tuning for each type of sequence, though $m1_{thresh} \approx 0.01$ has been found to be a good selection for the test cases used here.

8.3.3 Switches

Often, certain features of the matching process may not apply to the current video scene. In these cases it is useful to be able to customise the matching procedure, using switches, so that unnecessary computation and unrealistic assumptions are not applied. The switches for POD system are defined as follows:

(SWm_x, SWm_y)**:** These are each a 4×1 binary vector stipulating which measurements are to be calculated for each set of horizontal and vertical divisions.

$(SWint_x, SWint_y)$**:** Binary values determining whether any horizontal or vertical interference adjustment should be attempted.

The main source of differences is caused by the camera pose with respect to the tracking environment. When the camera shows a perspective view of a scene, people and objects generally occlude each other vertically depending on their distance from the camera (as is the case in test cases 1 and 3 further on). In this situation the vertical measurement ranges will often overlap while the horizontal measurements will provide separation. This means that measurements such as proportionality and interference adjustment will only work along one image direction.

A second scenario is when the camera is orientated perpendicular to the tracking ground plane (such as the ceiling cameras in test case 2). Here information will be

available in two dimensions so all measurements will provide consistent information. However in this case, the interference adjustment will block multiple objects from existing in a single strip and therefore should not be used.

Deciding which features to activate or deactivate is thus very intuitive and simply allows more flexibility when working with a variety of scene types.

8.4 Test Case 1: An outdoor environment

(a) Camera 1 (b) Camera 2

The first test case is a four person outdoor scene which was recorded with two Sony camcorders in an exterior environment. Table 8.1 below summarises the particulars of the sequence. Owing to the relatively small occlusion complexity in the scene, the perceptual complexity rating has been calculated to be fairly low. The second camera view has a very different dynamic lighting range causing blueish tint to be added to the foreground scene and therefore requiring colour correction. It should be noted that the test set size shown is the combined total frame count for both cameras. Lastly, the use of fixed cameras allows background removal using segmentation.

Perceptual Complexity (PC)	0.394
Number of cameras	2
Number of people	4
Image resolution	360 × 240
Running time	30 seconds
Training samples per person	4 frames
Total test set size	306 frames
Total ground truth set size	306 frames
Motion segmentation	yes

Table 8.1: *Scene Information*

8.4.1 Training

In the cartoon example shown previously, it was desirable to select training parameters that produced a number of colour classes which closely matched the characters' visual profiles. In a real-world system, however, there is much greater variance in a person's visual profile both temporally and spatially. For this reason, it is better to use a smaller σ_{train} so that more detail can be captured. Table 8.2 shows the parameters selected for training.

Parameter	Value
σ_{train}	5
k_{train}	1
nk_{train}	2
a_{thresh}	1

Table 8.2: *Selected training parameters*

Since the objective of the POD system is to correctly match a person's colour profile between multiple views, training samples are only drawn from one camera and then subsequently matched in either view. In this case, four samples of each person from Camera 1 make up the training set. Figures 8.11 and 8.12 show the set of trained people and their respective colour models.

The fact that Person 4 has been incorrectly characterised by light blue colours when his shirt is actually white shows that training should be applied to as large a mask as possible to ensure that camera CCD and lighting noise do not interfere excessively with the training process.

8.4.2 Colour correction

Since the presence of the bright sunlit area in the background of Camera 2 affects the colour distribution of the foreground, colour correction is necessary in order to ensure consistence of the trained colour models between views. It was found that direct application of the correction method described in chapter 5 does not provide stable

(c) Person 1 (d) Person 2 (e) Person 3 (f) Person 4

Figure 8.11: *Training Set*

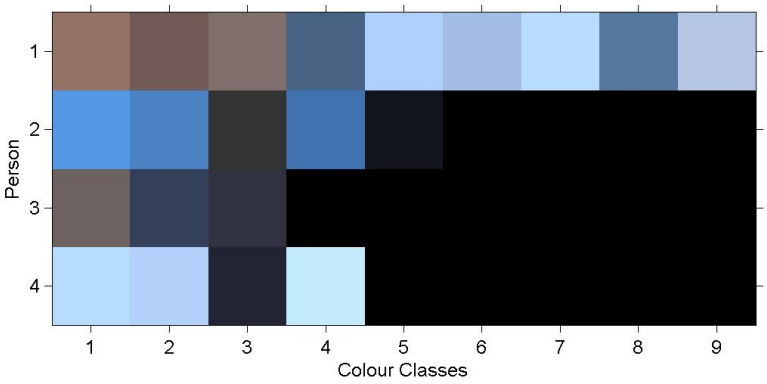

Figure 8.12: *Trained colour models for training set.*

results when significantly different areas exist between the camera views. Therefore, in order to obtain reasonable correction, the user must manually crop each image so that unrelated areas are not included when calculating the SOM representations. Generally, this involves selecting areas in each image view which fall well within the dynamic range of the camera. For instance, the sunlit background in Camera 2 should not be included when performing colour correction.

The correction coefficients calculated for the second camera are shown in Table 8.3.

Channel	x^1	x^0
Red	0.9967	4.3227
Green	1.0300	10.0175
Blue	0.9744	10.6950

Table 8.3: *Colour correction coefficients for Camera 2*

8.4.3 Matching

The matching parameters used for testing are shown below in Table 8.4. In concordance with the results discussed for tuning the parameters, σ_{match} has been kept the same as for training while k_{match} has been enlarged to account for greater variance. Since it is expected that the colour variance will still be substantial even with correction, the matching threshold $m1_{thresh}$ has been increased so that spurious errors are removed. Additionally, the area threshold $m2_{thresh}$ has been decreased to cope with the fragmentation of detected objects. Thus in the second camera the system is configured to require a closer match, but the matched region can be smaller.

The measurement switch vectors (SWm_x, SWm_y) have been set to apply all measurements, and model interference filtering $(SWint_x, SWint_y)$ has been enabled for the horizontal image direction. This is appropriate the scene since occlusions take place vertically.

Parameter	Camera 1	Camera 2
σ_{match}	5	same
k_{match}	2	same
(dx, dy)	[55, 55]	same
$(\sigma_{dx}, \sigma_{dy})$	[0.2, 0.2]	same
$m1_{thresh}$	0.01	0.02
$m2_{thresh}$	50	30
(SWm_x, SWm_y)	([1 1 1 1], [1 1 1 1])	same
$(SWint_x, SWint_y)$	[1, 0]	same

Table 8.4: *Matching Parameters*

8.4.4 Overall Results

Using the performance metrics described in Section 8.1.1, Table 8.5 summarises the average system performance for both camera sequences. In order to gauge the performance of the system relative to the colour correction process, the results show the breakdown for each camera view and, for comparison, include the case where no colour correction is applied to the second view. The overall result column represents the average ratings of both cameras excluding the uncorrected case.

In general, the overall detection performance is fairly high as shown by the Tracker Detection Rate (TRDR). Additionally, the low False Alarm Rate and alignment errors confirm this.

The Object Area Error (OAE) relating to the ratio of sizes between the ground truth and matching bounding boxes is slightly negative indicating that the matched areas tend to be 5% smaller than the actual object. This is due to the legs of Person 1, which are skin coloured, being matched very poorly. Since skin colour is fairly common across the scene, it will undoubtedly be assigned a low importance weighting and thus mostly be ignored by the matching process.

It is evident from the results that though a vast improvement in system performance is obtained by applying colour correction, there is a significant drop in system accuracy in the second camera. This is attributed to the fact that the colour correction is not

Rating	Overall	Camera 1	Camera 2	Camera 2 (without correction)
TRDR	0.89	0.97	0.81	0.35
FAR	0.025	0.00	0.05	0.05
OTE	0.15	0.06	0.23	0.66
OAE	-0.05	0.01	-0.11	-0.57
Processing rate	2.8 fps	2.8 fps	2.3 fps	2.8 fps

Table 8.5: *Overall test results*

perfect. In addition the online adaptation is explicitly not used so that true system performance is measured rather than a biased result due to the adaptation process.

Figure 8.13 shows the exact Track Detection Rate (TDR) for each modelled person in the scene. From the graphs, it can be seen that Persons 2 and 3 contribute to most of the system error, though Person 3 having dark colour is least affected by the environmental changes in the second camera view.

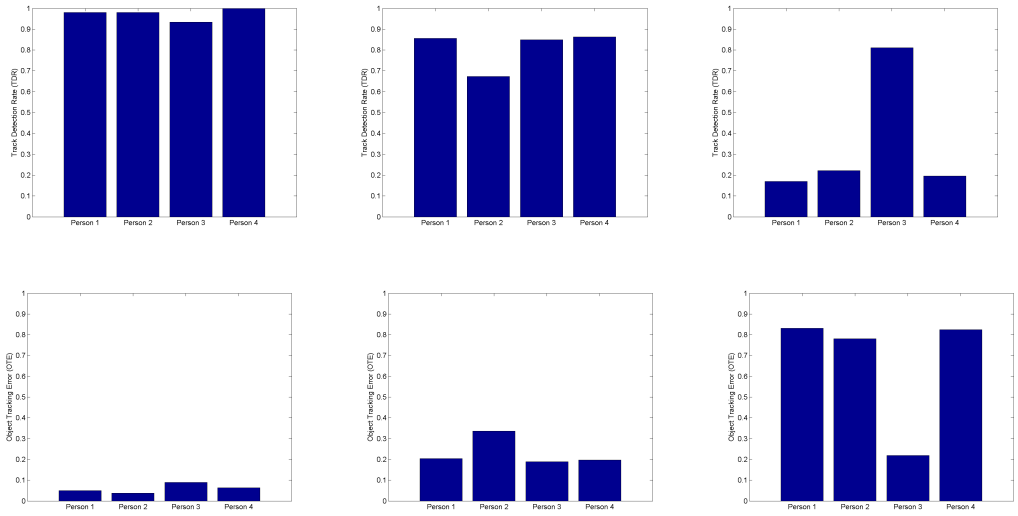

(a) Camera 1

(b) Camera 2 (with colour correction)

(c) Camera 2 (without colour correction)

Figure 8.13: *Track Detection Rate (TDR) (top); and Object Tracking Error (OTE) (bottom) for each person.*

A more descriptive relation between the object models is shown in the set of confusion matrices in Figure 8.14. These surfaces show the inter-class interference for all object

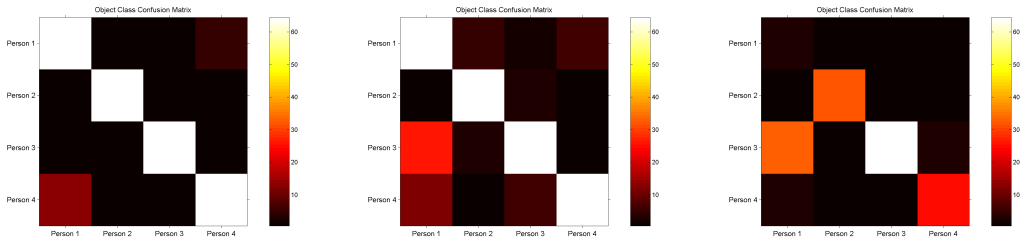

(a) Camera 1

(b) Camera 2 (with colour correction)

(c) Camera 2 (without colour correction)

Figure 8.14: *Object Model Confusion Matrices*

models. An ideal system with no inter-class interference would show maximum values along the diagonal of the matrix, similar to the matrix shown in Figure 8.14(a). The higher the value, the greater the number of hits for the two classes in question. From the confusion matrices, it can be seen that Persons 1 and 4 are sometimes confused. This is not surprising since they both have white shirts. The high confusion of Person 1 and Person 3 in the second camera is attributed to the end of the sequence where a major set of occlusions on the side of the image caused a large number of errors.

Finally, in order to provide a graphical view of the actual system error, example matched and ground truth trajectories have been plotted for Persons 1 and 2 in Figure 8.15. The complete set of trajectory plots can be found in Appendix C. These trajectories represent the centres of the bounding boxes for the ground truth and matched areas respectively. The purpose of the POD system is to make a spatial estimate of a particular object's position in an image irrespective of temporal information. This gives the system the ability to recover from errors that would otherwise cause a tracking system to become unstable.

For the purpose of illustration, the trajectory plots show the actual matched positions by means of plotted triangles. The plotted trajectories are then constructed by using

a 5-point moving average filter which remove spurious errors in the object's track. An example can be seen in Person 1's track (which is confused occasionally with Person 4) where the matched position erroneously shifts between two different people while the matched trajectory smoothly follows the ground truth. From the matched trajectories one can see that Persons 2 and 3 have the best matches with respect to the ground truth.

The improvement due to the incorporation of temporal information illustrates how the POD system could be used by other systems for recovery from failed tracking. As the POD system is designed to make instantaneous decisions about an object's location, it does not need to process every frame. Thus ideally, a fast time-dependent tracker could operate unencumbered and only use the POD at appropriate times (i.e. when its confidence is low). Since the primary objective of this work involves investigating the uses of colour in tracking, these applications have been left to future work.

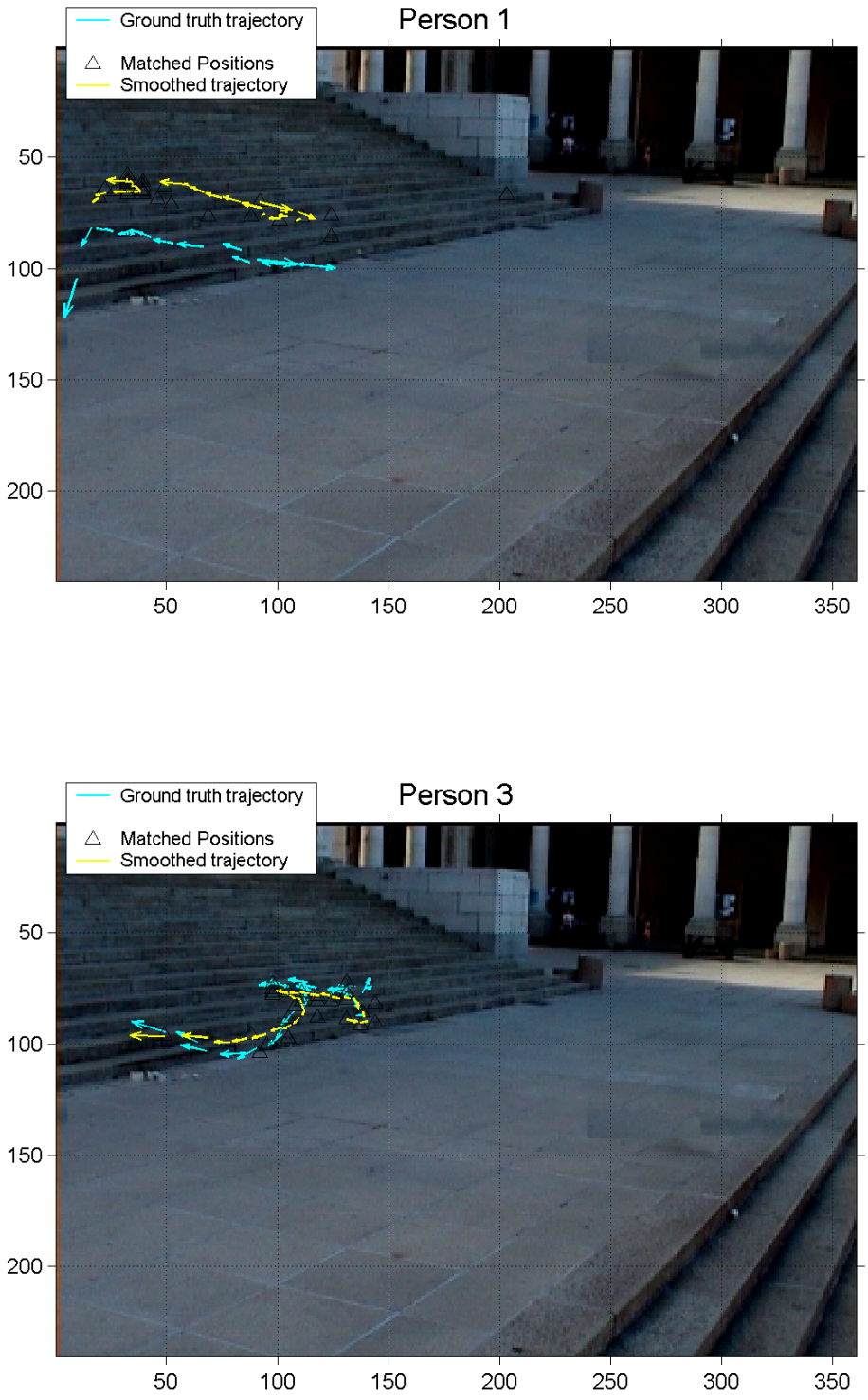

Figure 8.15: *Example trajectories for Persons 1 and 2 in Camera 1*

8.5 Test Case 2: An indoor CCTV system

This sequence consists of a total of seven coloured people entering and walking around a room[4]. Although the scene is indoors, there is a fair degree of variance close to the camera caused by the lighting arrangement, which causes certain people's shoulders to appear whiter when directly exposed. Motion segmentation is available since the camera position is fixed, however, because there is only one camera view, colour correction is not used. In terms of perceptual complexity, the people are more visibly different in appearance (lowering the Colour Similarity factor (CS)). However, the Occlusion Complexity (OC) is very high, contributing to the higher rating. Table 8.6 summarises the sequence's details.

Perceptual Complexity (PC)	0.549
Number of cameras	1
Number of people	7
Image resolution	384×288
Running time	90 seconds
Training samples per person	4 frames
Total test set size	464 frames
Total ground truth set size	464 frames
Motion segmentation	yes

Table 8.6: *Scene Information*

[4]Sequence courtesy of TSS Technology (De Beers).

8.5.1 Training

As with Test Case 1, a lower σ_{train} value is used to ensure a good spread of colour classes for the object models. Table 8.7 shows the training parameters, which are actually identical to the values used for Test Case 1.

Parameter	Value
σ_{train}	5
k_{train}	1
nk_{train}	2
a_{thresh}	1

Table 8.7: *Selected training parameters*

Figure 8.16 shows a sample of each person in the training set while Figure 8.17 shows each person's set of trained colour centres. The fact that Person 4 (White) has no other distinguishing colours implies that his profile is likely to become confused with some of the lighter-coloured people.

8.5.2 Matching

Matching parameters are similar to those selected for the previous test case. The differences include a high number of divisions (dx, dy) and narrower corresponding widths $(\sigma_{dx}, \sigma_{dy})$. This is chiefly in order to provide a finer distinction for dealing with the close proximity of the people and occlusions in the scene.

Additional tweaking includes the disabling of the proportion measurement in the SWm_y vector. Since the people in the scene can become large when near the camera, including the proportion measurement with such a number of divisions would cause decreased accuracy. Once again occlusions generally occur vertically, allowing interference $(SWint_x, SWint_y)$ filtering in the horizontal direction to be of use.

(a) Person 1 (Orange) (b) Person 2 (Red) (c) Person 3 (Green) (d) Person 4 (White)

(e) Person 5 (Blue) (f) Person 6 (Purple) (g) Person 7 (Yellow)

Figure 8.16: *Training Set*

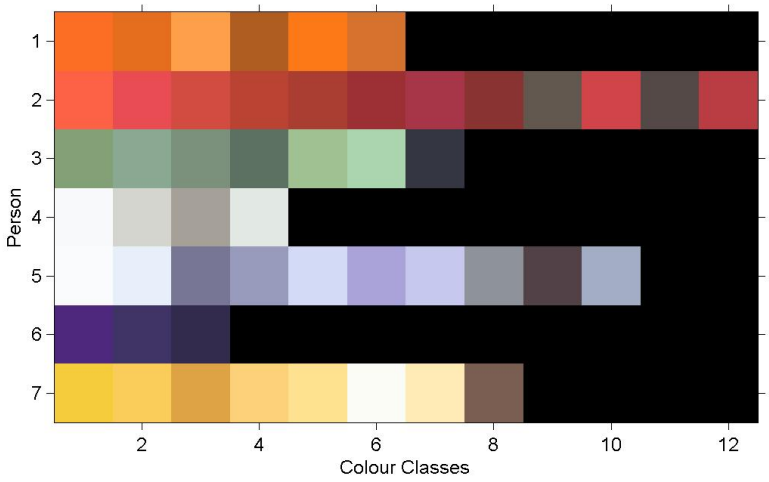

Figure 8.17: *Trained colour models for training set.*

Parameter	Camera 1
σ_{match}	5
k_{match}	2
(dx, dy)	[80, 80]
$(\sigma_{dx}, \sigma_{dy})$	[0.1, 0.1]
$m1_{thresh}$	0.01
$m2_{thresh}$	30
(SWm_x, SWm_y)	([1 1 1 1], [1 1 1 0])
$(SWint_x, SWint_y)$	[1, 0]

Table 8.8: *Matching Parameters*

8.5.3 Overall Results

In general the system seems to be able to handle the virtual continual occlusions present throughout the sequence. There were some problems (as anticipated) with Person 4 whom did not have sufficient colour diversity to be separated from other white areas. Once again the OAE (Table 8.9) reveals a tendency for the matched bounding box to be smaller than the actual person. In addition, the OTE is much larger than that of Camera 1 in Test Case 1. This is attributed to size mismatches caused by the larger scaling range present (i.e. the range of person sizes is greater in this sequence).

Rating	Overall
TRDR	0.85
FAR	0.00
OTE	0.16
OAE	-0.18
Processing rate	1.8 fps

Table 8.9: *Overall test results*

Two significant positive results are that the False Alarm Rate (FAR) is negligible and the processing rate does not drop excessively with the addition of more people. The reason for this is that the matching method processes all object models as a batch, thereby reducing the cost per model.

In terms of per person error, Figure 8.18 summarises the Track Detection Rate, Object Tracking Errors and confusion for each person.

Interestingly, Persons 3 (Green) and 7 (Yellow) have the poorest TDR and OTE ratings. Analysis of the sequence shows that the green person is occluded much of the time, and when parts of him are visible they are not detected since several other objects in front take precedence. Person 7, on the other hand, only enters the scene towards the end and does not have a chance to move around much. Therefore it is difficult to say whether the matching failures are due to his colour profile (which does overlap with those of Persons 1 and 4) or whether his errors are just averaged over too short a time.

On the confusion frontier, the largest conflict is due to the expected similarity between Person 4 (White) and Person 5 (Blue). Without temporal tracking or some other spatial features, this sort of problem cannot be solved directly by the POD matching system. Therefore this serves to illustrate the type of limitations inherent in the sole use of colour as a discriminator.

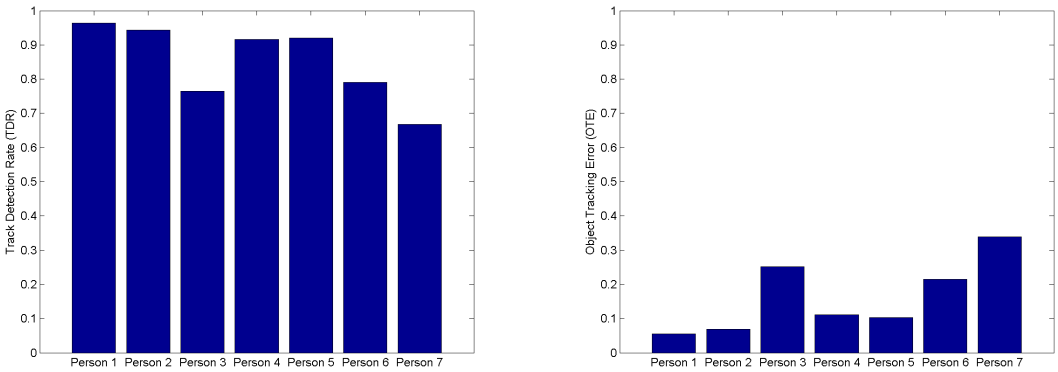

(a)

(b)

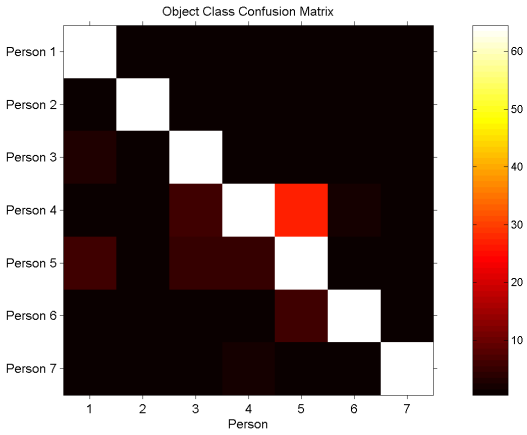

(c)

Figure 8.18: *(a) Track Detection Rate (TDR); (b) Object Tracking Error (OTE); (c) Object Model Confusion Matrix*

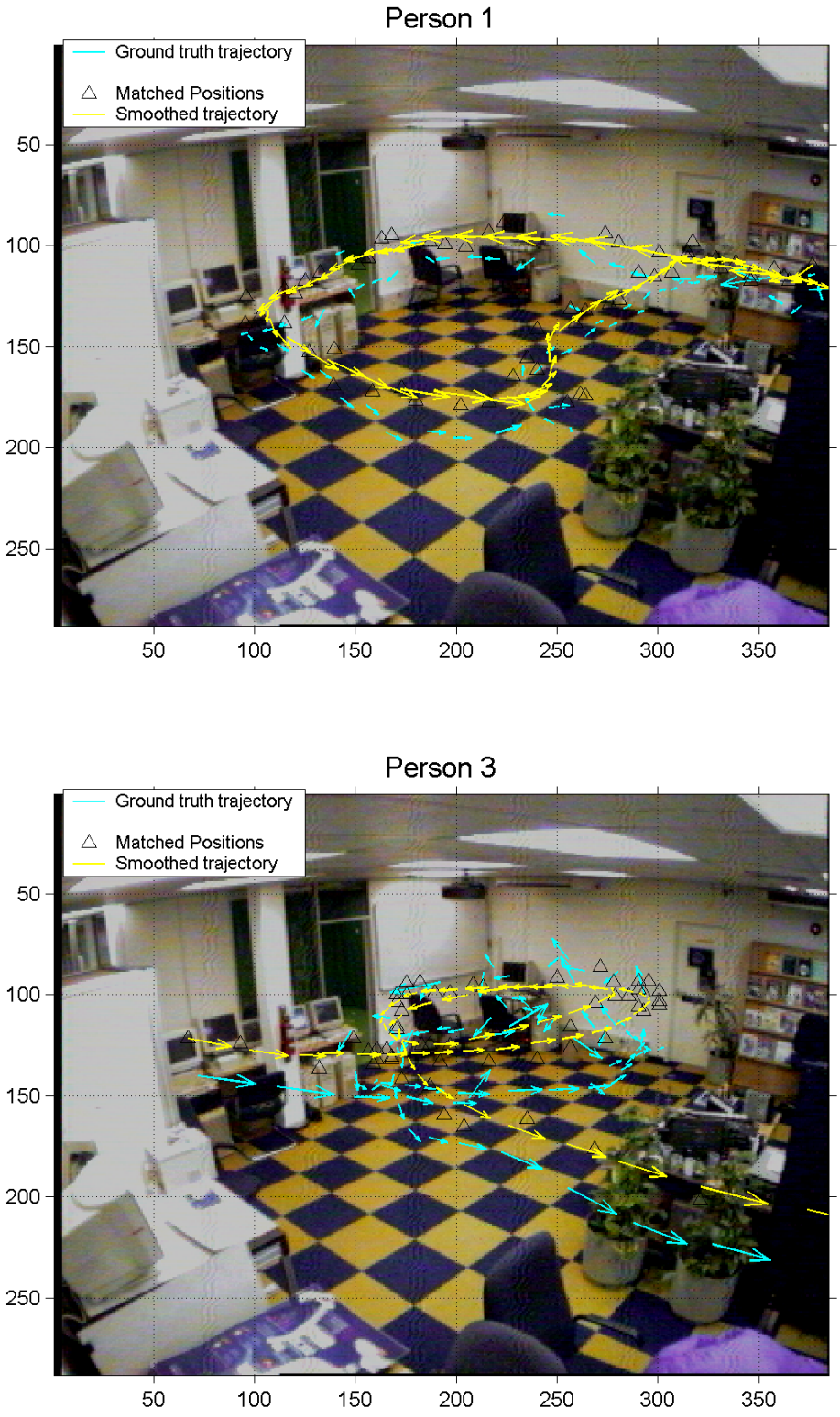

Figure 8.19: *Example trajectories for Persons 1 (Orange) and 3 (Green)*

8.6 Test Case 3: Surveillance using ceiling cameras

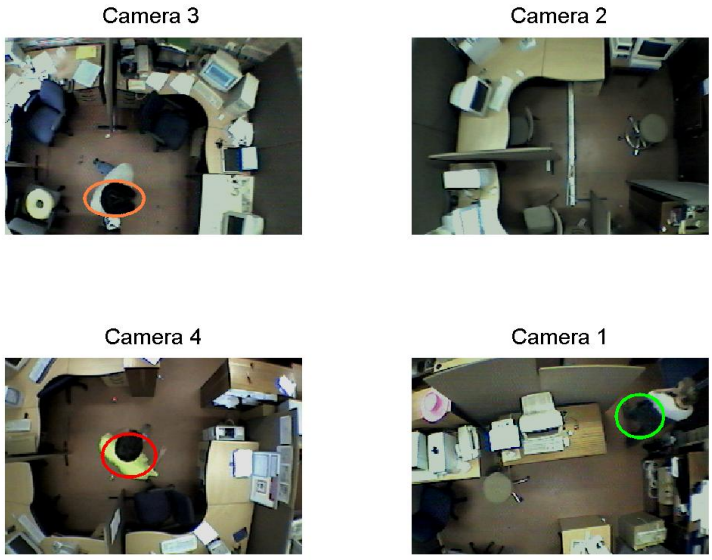

The final pre-recorded sequence used for testing consists of four ceiling-mounted cameras observing three people moving in a lab environment. The sequence was created in an asynchronous manner by four different computers. In order to simulate the effect of a video network, the entire quartet of cameras is processed iteratively in order of frame time stamps. The results shown are therefore the combined ratings for the system treated as a whole.

In terms of perceptual complexity, this sequence has been rated the highest with respect to the other test cases. Although the Occlusion Complexity (OC) is fairly low due to the nature of the ceiling cameras, the Colour Similarity (CS) between the people is much higher. The sequence is additionally complicated by the poor image quality. Owing to the large number of frames in the image (and the slow pace of action), ground truth was only created for every tenth frame. A final difficulty is the fish-eye lenses fitted to the ceiling cameras. These allow for a wide viewing range, but objects at the extremities of the frame are heavily distorted and are only partly

Perceptual Complexity (PC)	0.622
Number of cameras	4
Number of people	3
Image resolution	285×189
Running time	200 seconds
Training samples per person	2 frames
Total test set size	3798 frames
Total ground truth set size	354 frames
Motion segmentation	yes

Table 8.10: *Scene Information*

visible. For this reason, the input frames are cropped so that only the well-focused areas are processed. Table 8.10 shows the scene information. The end result is a scenario that is typical of a realistic surveillance network.

8.6.1 Training

Training parameters, shown in Table 8.11, are the same as for the two previous test cases.

Parameter	Value
σ_{train}	5
k_{train}	1
nk_{train}	2
a_{thresh}	1

Table 8.11: *Selected training parameters*

Camera 4, having the least variance, was chosen as the base view for training samples. The similarity between Persons 1 and 3 is evident from the respective images shown in Figure 8.20 and the trained colour profiles depicted in Figure 8.21. Their main differences are their hair colour and the fact that Person 1 has blue jeans. Unfortunately, the small size and low quality of image regions close to the floor makes it impossible for training to focus on this.

(a) Person 1 (b) Person 2 (c) Person 3

Figure 8.20: *Training Set*

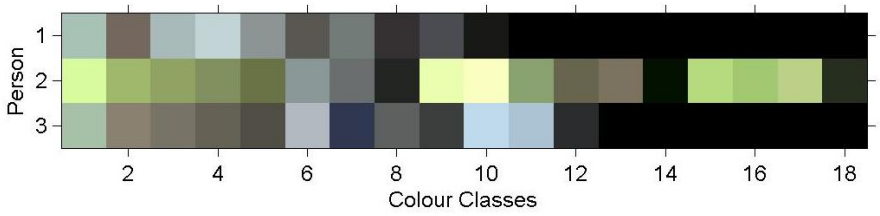

Figure 8.21: *Trained colour models for training set.*

8.6.2 Colour correction

Colour correction for this scene is interesting since each view is fairly similar. In fact, it was found that using the same coefficients to relate each of the three cameras to the training base (Camera 4) provided good correction. Table 8.12 shows the calculated coefficients. Since Camera 4 is much darker, the x^1 values are slightly less than 1 while the red/yellow highlights are compensated by the x^0 offsets.

Channel	x^1	x^0
Red	0.9408	-17.4685
Green	0.9820	-14.2080
Blue	0.9016	-6.2726

Table 8.12: *Colour correction coefficients for Cameras 1, 2 and 3*

8.6.3 Matching

A fundamental difference with ceiling cameras is that inter-person occlusions are not as noticeable. In fact, occlusions are mostly caused by people being occluded by a part of their surroundings. Additionally a person's visual profile tends to be similar in both the horizontal and vertical image directions. Therefore parameter selection for this scene, shown in Table 8.13, includes the use of all measurements (SWm_x, SWm_y) in both directions, and the omission of interference filtering. Since interference filtering $(SWint_x, SWint_y)$ will block multiple objects from occupying the same division, it cannot be activated without causing conflicts between several objects sharing an orthographic path.

Parameter	**Camera 1**
σ_{match}	5
k_{match}	2
(dx, dy)	[55, 55]
$(\sigma_{dx}, \sigma_{dy})$	[0.1, 0.1]
$m1_{thresh}$	0.005
$m2_{thresh}$	50
(SWm_x, SWm_y)	([1 1 1 1], [1 1 1 1])
$(SWint_x, SWint_y)$	[0, 0]

Table 8.13: *Matching Parameters*

The likelihood threshold $m1_{thresh}$ has been lowered in order to account for the high image variance (due to low image quality) and the fact that colour correction is not precise. This setting is balanced by increasing the area threshold $m2_{thresh}$. The area threshold is especially useful in this scene because object sizes are generally constant in the ceiling camera views.

8.6.4 Overall Results

The decreased performance rating shown by the TRDR in Table 8.14 is primarily due to the high similarity between Persons 1 and 3. Although the system is able to

distinguish the two models under good conditions, the presence of overhead fluorescent lights causes overexposure of each person's shoulders in certain places. Thus even Person 2 has a fairly low detection rate when in Camera 2's view.

Rating	**Overall**	**Overall (without colour correction)**
TRDR	0.76	0.67
FAR	0.03	0.03
OTE	0.24	0.33
OAE	-0.23	-0.33
Processing rate	3.8 fps	3.8 fps

Table 8.14: *Overall test results*

The perceived similarity between the camera views is confirmed by the results shown for the uncorrected case, which are fairly close. The fact that the FARs are identical show that the even without colour correction there are relatively few false positive hits. Therefore the colour correction serves to improve object detection in this case.

Failures aside, the False Alarm Rate (FAR) is still fairly low even with the lowering of the likelihood threshold $m1_{thresh}$. Another good result is the processing rate which encompasses the entire operating speed for the whole camera network in parallel (computed on the single test platform).

Bar graphs in Figure 8.22 show the Track Detection Rate (TDR) and Object Tracking Error (OTE) values obtained for each person for both the colour corrected and uncorrected cases respectively. To reiterate, owing to the image colour similarities, the results are close. Intuitively, Person 2, having a distinguishable yellow shirt, is tracked best. The errors due to the similarity of Persons 1 and 3 are further evident from the confusion matrices shown in Figure 8.22. Although the confusion is less for the uncorrected case, it should be realised that this is because the object detection is lower.

An example trajectory for Person 2 is shown in Figure 8.23. In Camera 1, no matches are found due to the heavy occlusions of surrounding partitions. His track for the other views, however, remains close to the ground truth path.

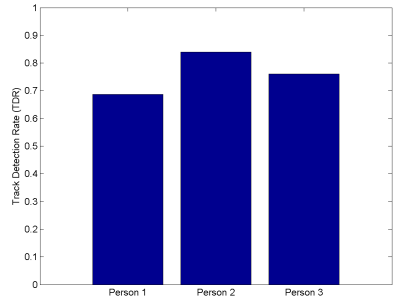

(a) Colour Corrected

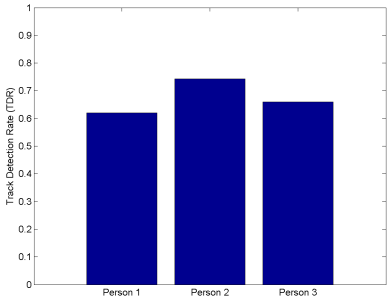

(b) Uncorrected

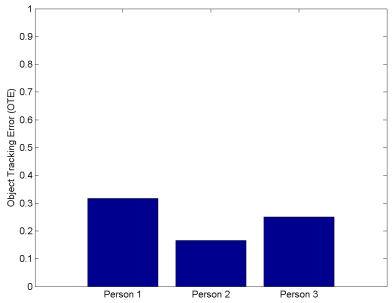

(c) Colour Corrected

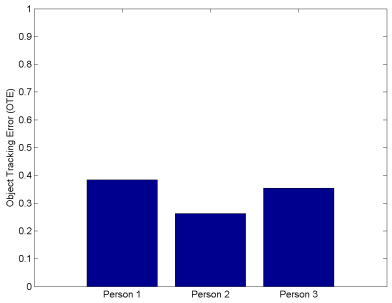

(d) Uncorrected

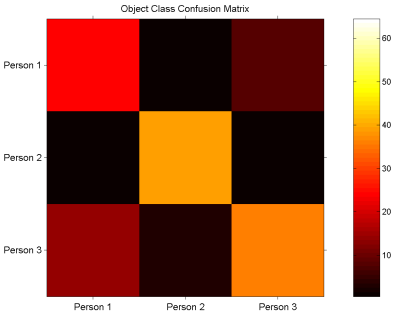

(e) Colour Corrected

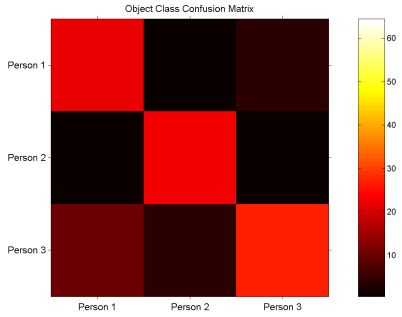

(f) Uncorrected

Figure 8.22: *(a),(b) Track Detection Rate (TDR); (c),(d) Object Tracking Error (OTE) (e),(f) Object Model Confusion Matrix.*

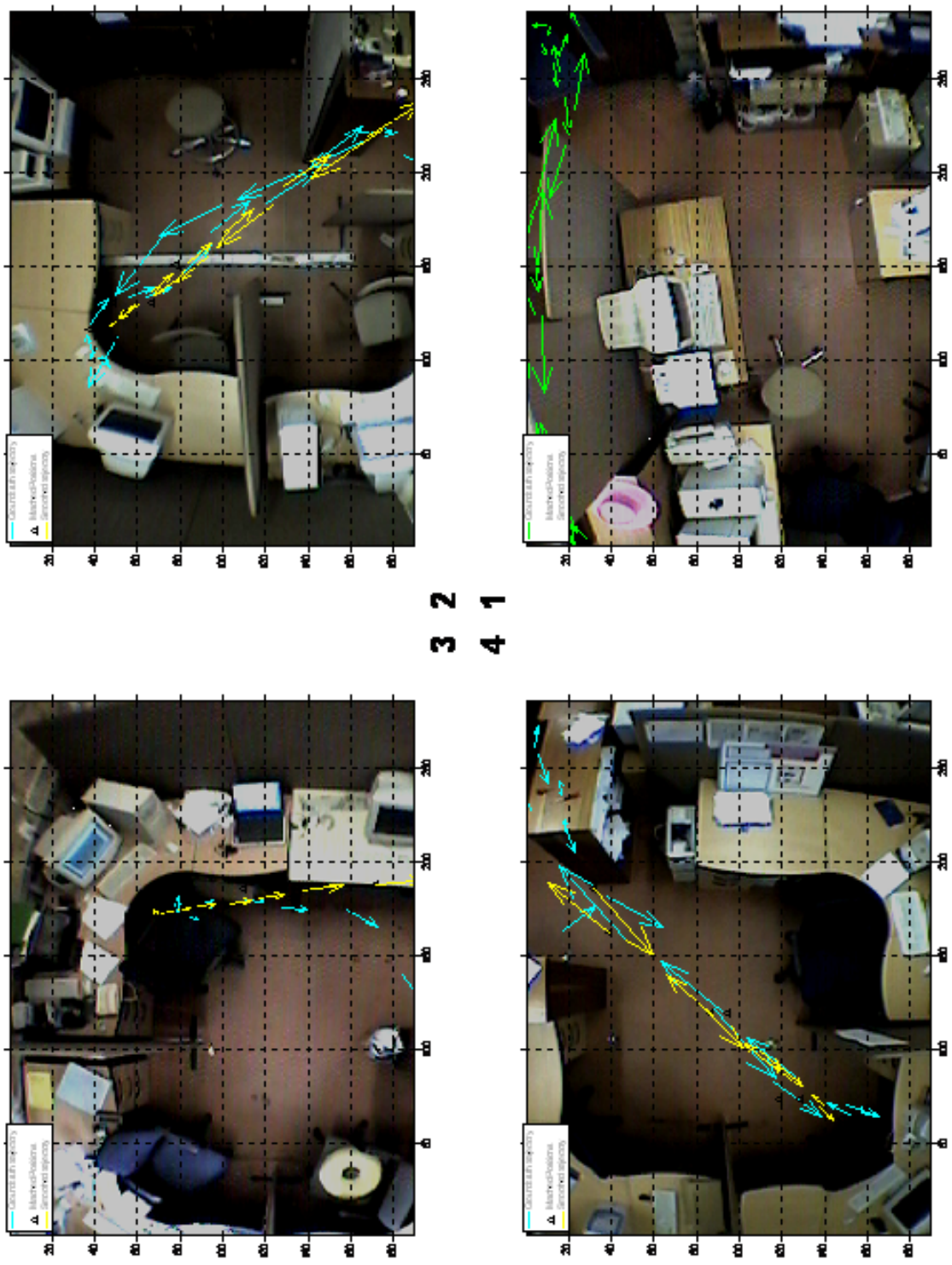

Figure 8.23: *Overall trajectory for Person 2.*

8.7 Discussion

From the test cases, it is seen that the POD system is able to distinguish several people based only on colour information provided that there is enough variety in the trained models. There is a tendency for detected areas to be slightly smaller than the actual object. This has been attributed to the fact that lower object extremities are generally occluded by surrounding objects and shadows. This leads to the regions being filtered out either by the initial motion segmentation or the colour matching steps. The result is a smaller, raised bounding box.

The system proves to be robust through a number of differing camera environments and is not overly sensitive to parameter tuning. A beneficial aspect of the system is that it provides a realisable distributed framework which can be flexibly integrated with a variety of other systems. Its ability to make an instantaneous decision about any trained object allows it to cope with asynchronous video feeds and recovery from occlusions. By additional incorporation of temporal history, it has been shown in the presented test cases that a smooth trajectory can be extracted from a classified set at any time.

8.7.1 Overall Ratings

In order to assess the overall system performance, the results of each test case are compared, using their Perceptual Complexity (PC) as a relative basis. Figure 8.24 summarises the Tracker Detection Rates (TRDR) for the test cases.

As expected, the TRDR decreases as the PC increases. Unfortunately, without more test sets with high PC ratings, it is impossible to know the exact lower error bound of the system. Figure 8.24 also shows the average Object Tracking Error (OTE) for each sequence. The fact that the OTE seems to complement the TRDR confirms the fact that the TRDR is a truthful value. For instance, were a true positive hit acquired with a very large OTE, it would imply that the wrong object had accidently caused

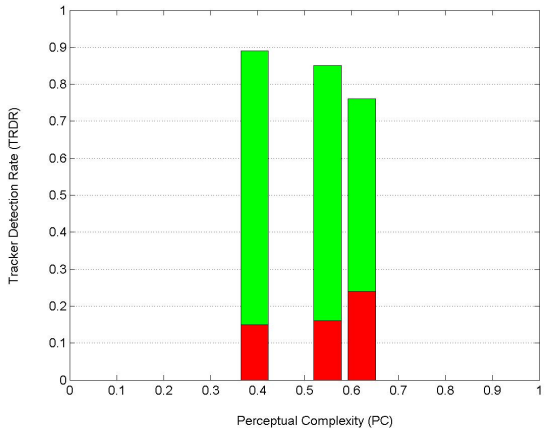

Figure 8.24: *Overall TRDR (upper green) and OTE (lower red) ratings for all test cases.*

the detection rather than the actual one. Therefore this summarises the fact that, in general, the overall confusion between object classes is fairly low for the given test cases.

Finally, the False Alarm Rate (FAR) of the system is on average just below 2% with a mean processing rate of approximately 3 fps. The processing rate is not heavily affected by an increase in the number of trained objects. More elaborate optimisation of the current implementation could result in much faster frame rates.

8.7.2 Segmentation

An interesting development in the system was the effect of using different motion segmentation processes. In Chapter 4, a comprehensive segmentation algorithm was implemented in order to optimise the quality of segmentation. However, owing to the robustness of the matching algorithm, it was found that, in practice, using a single threshold basic background subtraction process (initially condemned in Chapter 4) provided very little degradation in system performance while simultaneously increasing the system's overall processing speed.

8.7.3 Colour Correction

Quantifying the overall performance of the colour correction method is difficult, given the abstract nature of the process. Although comparative CIELAB values could be used to describe the improvements (as was done in Chapter 5), this means very little when considering the system performance as a whole.

Based on the test cases (specifically Cases 1 and 3), there is approximately a 35% improvement when applying the method depending on the lighting characteristics of the scene.

8.7.4 Online Adaptation

It is important to note that while the POD system is able to adapt the colour models, this feature was not used for the test cases. Owing to the fact that the sequences are relatively short, it was thought that allowing adaptation would not significantly improve performance. Additionally, any improvement due to the adaptation would then mask the true performance of the matching process. Online adaptation has been dealt with extensively for Gaussian mixture models [26] and is known to improve long-term tracking. Thus the POD system can apply adaptation for situations in which there is more temporal variance.

Chapter 9

Concluding Remarks

A system capable of using the colour appearance of objects and people to detect their position within a digital video surveillance network has been presented. The system suggests a distributed, bottom-up implementation which can easily be integrated with off-the-shelf network products.

Features of the system include:

- Independence from camera pose and position
- Ability to deal with asynchronous video connections
- Persistence of object models over a distributed camera network
- Flexibility of integration with other visual tracking systems.

9.1 System summary

A bottom-up approach has been applied and each processing stage is fully modularised. Pre-processing consists of motion and colour segmentation, and a colour correction method for dealing with multiple views. System operation then proceeds

in a two-stage process consisting of training and matching. Training involves representing objects as colour Gaussian mixtures which are then matched using a batch analytical method. While the implementation is equipped to perform online adaptation of the models, the test sequences are not very long. Thus it was thought that not using adaptation would provide a clearer view of the system's actual performance.

Some basic surveillance metrics have been applied in order to assess the performance of the system. An average accuracy of approximately 80% is achieved for overall system performance, though the exact performance is inversely proportional to the perceptual complexity[1] of the scene. The system exhibits a very low false alarm rate and is capable of an average processing rate of 3 fps with little dependence on the number of tracked objects. It is envisaged that further work may yield better optimisation with faster frame rates.

9.2 Future work

While current 3-D tracking systems obtain good results, a common weakness is their inability to recover from failure. Since the POD system is able to generate a hypothesis without being dependent on temporal priors, it is thought that the combination of the system with a 3-D tracker could produce a viable solution. One possibility is for the 3-D tracker to exploit the POD's ability to deal with asynchronous video by only presenting it with frames when the overall system confidence is low. Alternatively, the POD could be used full-time for providing a Kalman or particle filter with observations.

In such scenarios, several contingencies have been considered for training the POD system:

External: A simple approach would be to allow the 3-D tracker to train the POD system by forwarding its processed observations.

[1] Refer to Section 8.1.2.

Internal supervised: If the 3-D tracker is unable to initialise from the start, training can be achieved by presenting the POD system with segmented frames. This would be most suitable for a large camera network in which people enter and leave a building through one of several confined exits. A profile camera view could then be used at these locations with a set of simple blob tracking (or silhouette detection) rules, to produce training data. Alternatively, if only some of the people need to be tracked, surveillance personnel can interactively select objects using a GUI.

Internal unsupervised: The original idea (which has not been completed) is to allow the POD system to track all encountered coloured regions as a single model (multiple matching can be allowed). Since the system considers all models as a batch, analysis of the trajectories of all colour centres over time could then be used in a split/merge scheme to slowly separate each person's model. This would yield a fully automated training procedure. However, further work is required in order to fully determine its viability.

While the system can be applied to assisting real-time tracking systems, it is also thought that the ideas presented may hold further application in automated image retrieval and robotic vision areas. It is hoped that further extension of this work combined with robust 3-D tracking systems such as [27] could lead to an eventual real-time solution.

Appendix A

SOM Training

The SOM toolbox for Matlab supports both sequential and batch training methods. In sequential training the input data points are handled independently, while the batch method presents all the data points to the map before any adjustments are made. The batch method, being far more efficient, is the default method used by the toolbox and is outlined below [43]:

Firstly, d-dimensional neurons are chosen as low dimensional map units $\mathbf{m} = [m_1, ..., m_d]$ and the n-dimensional input vectors $\mathbf{x}$ are applied.

Partitioning of the data according to the Voronoi regions of the map weights proceeds for each epoch (training step). This assigns each input vector to its nearest neuron and updates the weighting using a K-means-like approach:

$$m_i(t+1) = \frac{\sum_{j=1}^{n} h_{ic}(t)\mathbf{x}_j}{\sum_j = 1^n h_{ic}(t)}, \tag{A.1}$$

where $c = \text{argmin}_k\{||x_j - m_k||\}$ is the index of the BMU (Best Matching Unit) of data vector x_j and $||.||$ is the distance measure, which is typically the Euclidean distance.

Each weight contributing to the final average is calculated from a neighbourhood function $h_{ic}(t)$, which defines the relation between neurons for every BMU c. If any component values are missing, they are simply ignored from the calculation of the weighted average. Figure A.1 illustrates the update process.

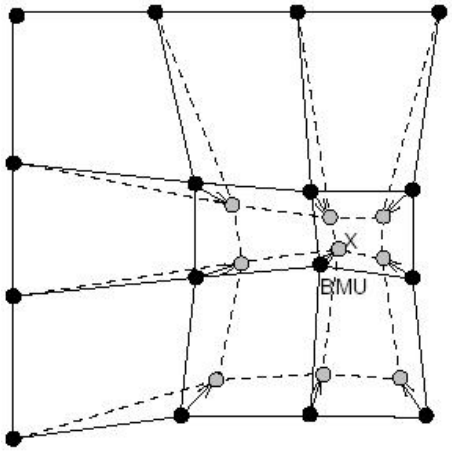

Figure A.1: *Updating the Best Matching Unit (BMU) and its neighbours for input vector* $\mathbf{x}$ *[43].*

The training progresses in two phases, rough and fine tuning. Rough tuning uses a fast learning rate to obtain a general fit of the neurons to the input vectors. Fine tuning then slows the learning rate, resulting in a more exact fit.

Termination of the training process is determined by specifying either the number of training epochs or an upper threshold for the overall quantisation error.

Appendix B

Test Platform Specifications

The specifications of the test platform used is tabulated below.

Processor	Intel Pentium IV 2.8 GHz
RAM Capacity	1024 MBytes
Video capture interface	FireWire / BT868 Compatible
Image format	bmp / png
Operating System	Windows XP 2002 SP1
Development Platform	Matlab 6.5 / MSVC++ 6

Table B.1: *Test Platform Specifications*

Appendix C

Digital Appendix

The items referenced here can be found on the accompanying CDROM. These include:

- Full thesis PDF document
- Processed test sequence results (compressed with Cinepak radius codec)
- Colour trajectory plots of each person for all test sequences.

Bibliography

[1] R. Adams and L. Bischof. Seeded region growing. *IEEE Transactions on Pattern Analysis and Machine Intelligence*, 16(6):641–647, June 1994.

[2] H. Austermeier, G. Hartmann, and R. Hilker. Color-calibration of a robot vision system using self-organizing feature maps. *ICANN*, pages 257–262, 1996.

[3] D. H. Ballard and C. M. Brown. *Computer Vision*. Prentice-Hall Inc., 1982.

[4] J. Black, T. Ellis, and P. Rosin. A novel method for video tracking performance evaluation. In *Joint IEEE International Workshop on VS-PETS*, October 2003.

[5] J. Brusey and L. Padgham. Techniques for obtaining robust, real-time, colour-based vision for robotics. In *Proceedings of the IJCAI-99 Third International Workshop on Robocup*, 1999.

[6] P. J. Burt, T. H. Hong, and A. Rosenfeld. Segmentation and estimation of image region properties through cooperative hierarchical computation. *IEEE Transactions On Systems, Man, and Cybernetics*, 11(12):802–809, 1981.

[7] D. Comaniciu, V. Ramesh, and P. Meer. Real-time tracking of non-rigid objects using mean shift. In *IEEE CVPR*, 2000.

[8] M. Dittenbach, D. Merkl, and A. Rauber. The growing hierachical self organising map. In *IEEE International Joint Conference on Neural Networks*, 2000.

[9] D. Doermann and D. Mihalcik. Tools and techniques for video performance evaluation. In *Proceedings of the Third International Workshop on Performance Evaluation of Tracking and Surveillance*, June 2002.

[10] R. O. Duda and P. Hart. *Pattern Classification and Scene Analysis*. Wiley-Interscience, 1973.

[11] C. Erdem, B. Sankur, and A. M. Tekalp. Metrics for performance evaluation of video object segmentation and tracking without ground-truth. In *IEEE International Conference on Image Processing*, October 2001.

[12] G. Finlayson and R. Xu. Illuminant and gamma comprehensive normalisation in log RGB space. *Pattern Recognition Letters*, 24(11):1679–1690, 2003.

[13] J. D. Foley, A. van Dam, S. K. Feiner, and J. F. Hughes. *Computer Graphics Principles and Practice Second Edition in C*. Addison-Wesley Publishing Company, 1992.

[14] A. Ford and A. Roberts. Colour space conversions. Technical report, 1998. [Online]. Available: http://www.poynton.com/PDFs/coloureq.pdf [January 2004].

[15] D. A. Forsyth and J. Ponce. *Computer Vision: A Modern Approach*. Prentice Hall, 2003.

[16] J. Geusebroek, R. Boomgaard, A. W. M. Smeulders, and T. Gevers. Color constancy from physical principles. *Pattern Recognition Letters*, 24(11):1653–1662, 2003.

[17] I. Haritaoglu, D. Beymer, and M. Flickner. Video-CRM: Detection and tracking people in stores. In *Joint IEEE International Workshop on VS-PETS*, October 2003.

[18] Intel. *Open Source Computer Vision Library Reference Manual*. Intel Corporation, USA, 2001. [Online]. Available: http://www.sourceforge.net/projects/opencvlibrary/index.html [February 2004].

[19] M. Isard and A. Blake. Condensation — conditional density propagation for visual tracking. *International Journal of Computer Vision*, 29(1):5–28, 1998.

[20] A. D. Jepson, D. J. Fleet, and T. F. El-Maraghi. Robust online appearance models for visual tracking. In *IEEE CVPR*, volume 1, pages 415–422, 2001.

[21] P. Kaewtrakulpong and R. Bowden. An improved adaptive background mixture model for real-time tracking with shadow detection. In *Proc. 2nd European Workshop on Advanced Video Based Surveillance Systems*, 2001.

[22] H. Kolb, E. Fernandez, R. Nelson, and B. W. Jones. The perception of color. Technical report, Webvision, 2003. [Online]. Available: http://webvision.med.utah.edu/KallColor.html [January 2004].

[23] A. Kosir and J. F. Tasic. Pyramid segmentation parameters estimation based on image total variation. In *Proceedings of IEEE conference EUROCON 2003*, 2003.

[24] T. M. Martinetz, S. G. Berkovich, and K. J. Schulten. Neural-gas network for vector quantization and its application to time-series prediction. *IEEE Transactions on Neural Networks*, 4(4):–569, 1993.

[25] S. J. McKenna, S. Jabri, Z. Duric, A. Rosenfeld, and H. Wechsler. Tracking groups of people. *Computer Vision and Image Understanding*, 80:42–56, 2000.

[26] S. J. McKenna, Y. Raja, and S. Gong. Tracking colour objects using adaptive mixture models. *Image Vision Computing*, 17:225–231, 1999.

[27] B. Merven, F. Nicolls, and G. de Jager. Multi-camera person tracking using an extended kalman filter. In *Fifteenth Annual Symposium of the Pattern Recognition Association of South Africa*, 2003.

[28] A. Mittal and L. S. Davis. M2tracker: A multi-view approach to segmenting and tracking people in a cluttered scene using region-based stereo. In *Computer Vision - ECCV 2002, 7th European Conference on Computer Vision, Copenhagen, Denmark, May 28-31, 2002, Proceedings, Part I*, 2002.

[29] I. Nabney and C. Bishop. Netlab neural network software. [Online] Available: http://www.ncrg.aston.ac.uk/netlab, [November 2003].

[30] K. Nummiaro, E. Koller-Meier, T. Svoboda, D. Roth, and L. V. Gool. Color-based object tracking in multi-camera environments. In *25th Pattern Recognition Symposium, DAGM 2003*, 2003.

[31] R. N. Pal and S. K. Pal. A review on image segmentation techniques. *Pattern Recognition*, 26(9):1277–1294, 1993.

[32] A. Rizzi, C. Gatta, and D. Marini. Color correction between gray world and white patch. In *Proceedings of SPIE*, volume 4662, pages 367–375, 2002.

[33] A. Rizzi, C. Gatta, and D. Marini. A new algorithm for unsupervised global and local color correction. *Pattern Recognition Letters*, 24(11):1663–1677, 2003.

[34] T. J. Roberts, S. J. Mckenna, and I. W. Ricketts. Adaptive leaning of statistical appearance models for 3D human tracking. In *BMVC*, 2002.

[35] P. L. Rosin. Thresholding for change detection. In *Proc. ICCV*, Jan 1998.

[36] A. Senior. Real-time articulate human body tracking using silhouette information. In *Joint IEEE International Workshop on Visual Surveillance and Performance Evaluation of Tracking and Surveillance*, October 2003.

[37] A. Silberschatz, H. F. Korth, and S. Sudarshan. *Database System Concepts*. WCB/McGraw-Hill, 3rd edition, 1999.

[38] P. Y. Simard, L. Bottou, P. Haffner, and Y. L. Cun. Boxlets: a fast convolution algorithm for signal processing and neural networks. In *Advances in Neural Information Processing Systems*, volume 11, pages 571–577. 1999.

[39] S. W. Smith. *The Scientist and Engineer's Guide to Digital Signal Processing*. California Technical Publishing, 1997.

[40] I. Sommerville. *Software Engineering*. Addison-Wesley, 5th edition, 1995.

[41] C. Stauffer and W. Grimson. Adaptive background mixture models for real-time tracking. In *Computer Vision and Pattern Recognition*, 1999.

[42] M. Tabb and N. Ahuja. Multiscale image segmentation by integrated edge and region detection. *IEEE Transaction on Image Processing*, 6(5), May 1997.

[43] J. Vesanto, J. Alhoniemi, and J. Parhankangas. SOM toolbox for Matlab 5. Technical report, Helsinki University of Technology, April 2000.

[44] P. Viola and M. Jones. Robust real-time object detection. In *Second International Workshop on Statistical and Computational Theories of Vision — Modeling, Learning, Computing, and Sampling*, 2001.

[45] G. Welch and G. Bishop. An introduction to the Kalman filter. Technical Report TR 95-041, Department of Computer Science, University of North Carolina, 2002.

[46] S. Westland. Frequently asked questions about colour physics. Technical report, Colourware, 2000. [Online]. Available: http://www.colourware.co.uk/cpfaq.htm [January 2004].

[47] G. Wyszecky and W. S. Stiles. *Color Science: Concepts and Methods, Quantitative Data and Formulas*. J. Wiley & Sons, New York, 1982.

[48] I. T. Young, J. J. Gerbrands, and L. J. van Vliet. *Fundamentals of Image Processing*. Delft University of Technology, Netherlands, 1995.

[49] Z. Yue, S. K. Zhou, and R. Chellappa. Robust two-camera tracking using homography. Accepted for 2004 IEEE International Conference on Acoustics, Speech, and Signal Processing, 2004.